Satellite Studies of Severe Convective Storms

Co-Principal Investigators:

David W. Reynolds
and
Thomas H. Vonder Haar

Department of Atmospheric Science
Colorado State University
Fort Collins, Colorado

NSF Grant No.: ATM 76-21307

Colorado State University

Department of Atmospheric Science

Paper No. 290

SATELLITE STUDIES OF SEVERE CONVECTIVE STORMS

By

David W. Reynolds and Thomas H. Vonder Haar

Co-Principal Investigators

Co-Authors by Section

2.0 Donald W. Hillger
3.0 Andrew J. Negri
4.0 Robert A. Maddox
5.0 David W. Reynolds

Department of Atmospheric Science

Colorado State University

Ft. Collins, Colorado

FINAL REPORT

NSF ATM76-21307

Atmospheric Science Section

June, 1978

ABSTRACT

Results are reported in the analysis of the pre-severe and severe storm environment using meteorological satellite data. Using polar-orbiter vertical temperature sounder data and applying statistical methods, determination of the scale and intensity of pre-severe storm temperature and moisture gradients have been examined. Results show that strong moisture gradients at the 100-200 km scale and temperature gradients at the 200-400 km scale are precursors to severe weather events.

Through the use of satellite derived low level wind vectors, combined with surface moisture values, results have shown some skill in relating areas of high moisture convergence with subsequent severe weather. These low-level wind vectors have also been used independently to derive low level convergence and vorticity patterns at the mesoscale in the pre-storm environment. A statistical examination was performed on the derived winds to examine their accuracy and the scale needed to be able to define the severe weather environment. These results show that the features of importance occur at two separate wavelengths, 150 km or less, and 600-800 km. Thus both mesoscale and synoptic scale forcing features are significant to severe weather development, at least on the days examined here. Once the severe weather has developed, the rate of growth of the cloud, as determined by decrease in cloud top temperature, is related to the timing of the severe weather event.

Preliminary results from a cloud climatology performed over Oklahoma for the April-June period using two years of SMS/GOES data are reported. The pre-convective cloudiness is examined during the morning hours (1000 LT) to determine how it effects satellite sounder capabilities and subsequent severe weather occurrence. On 41% of severe weather days, no satellite

sounder information could have been made due to overcast cloudiness. On the majority of the severe weather days examined, the convective clouds formed over the areas having morning cloudiness rather than in the clear air or at cloud-clear boundaries. This is explained by the fact that the clouds represent areas of moisture and vertical motion conducive to convective development.

TABLE OF CONTENTS

1.0 Introduction

The first year's effort under Grant ATM-76-21307 has concentrated on two main areas. The first concerns the study of the pre-convective environment using satellite sounder information. This study emphasized the ability of the satellite information to identify, in the x-y plane, mesoscale temperature and/or moisture discontinuities that might aid in the initiation of thunderstorm activity. Using statistical analysis methods (i.e. structure and correlation functions) the sounder data were analyzed to determine at what horizontal scales the atmosphere showed the most "structure" in terms of temperature and moisture. Using the closely spaced NSSL RAOB network, it was possible to compare the satellite sounder structure function analysis with those from the RAOB network. The comparisons lead to the conclusion that the sounder data can reproduce mean gradients which are similar to those sensed by conventional RAOB data. Further analysis showed some degree of skill in determining severe - non-severe weather days by looking at the magnitudes of the structure functions of temperature and moisture on these types of days. Future work will hopefully complement and extend the results reported to date.

As an offshoot of this work, a small study was performed to determine the pre-convective cloudiness on severe weather days. This study would determine whether satellite soundings could be made on these days, as well as the relationship of the cloudiness to subsequent severe weather. Results of this study are included in the report.

The second main effort was in using the digital image data from GOES-1 to determine the usefulness of this data in helping to understand and predict severe weather events. A concerted effort was made to determine

accurate low-level wind measurements using vectors derived from cloud motions. Not only were the normal kinematic analysis of low-level convergence and vorticity examined, but combinations of surface moisture and satellite sounding derived moisture were combined with these wind vectors to derive low-level moisture convergence. A secondary study, following along the lines of the satellite sounder analysis, involved the statistical structure of the wind vectors. This was done to help define the magnitude of the noise of the measurements and the measurement systems as well as to determine the different scales of motion in the data field. These types of studies are important if one is to have confidence in the satellite wind vectors and in their potential importance in weather analysis and forecasting.

Further investigations were made of the growth characteristics of several severe storms through use of the infrared data. Changes in cloud-top-temperature were monitored to see if any signatures could be identified to discriminate between severe and non-severe storms, and to determine the timing and location of the severe storm event. Five-minute interval digital data were used for both the above mentioned studies and were shown to be imperative to these studies.

Future work will concentrate on the analysis of 3 minute interval digital satellite data collected in the Spring of 1977. These studies will try to substantiate the work performed under this first year's work and should greatly aid in our understanding of severe local storms.

2.0 Analysis of Mesoscale Satellite Infrared Soundings Using Statistical Structure and Correlation Functions

2.1 Introduction

A statistical analysis of satellite infrared sounding data from the VTPR (Vertical Temperature Profile Radiometer) on NOAA-4 was performed using structure and correlation functions. Satellite radiances, retrieved temperatures, and moisture information in the form of radiance residuals were examined. The statistical structure functions for temperature at 500 and 700 mb were computed and compared to similar results computed for mesoscale rawinsonde temperature data. The mesoscale rawinsonde soundings were obtained during the National Severe Storms Laboratory (NSSL) data collection period in May and June of 1976. For this same period satellite soundings were retrieved on 14 of the mesoscale soundings days. The two data sets were also compared in terms of normalized correlation functions for moisture, using mixing ratios from rawinsonde data and radiance residuals from the satellite soundings.

The structure function analysis was also applied on an individual basis to each day in the data set. Structure functions for VTPR radiances for channels 6 and 7 were examined and compared to significant weather reports later that day. Mean temperature and moisture gradients in terms of structure function change with distance can be detected without conventional sounding information. Structure functions for 500 mb temperatures were also examined on a daily basis, but low level tropospheric temperature and moisture gradients seem to be the main precursors to most severe storm development.

2.2 Structure and Correlation Functions

Statistical structure and correlation functions were used by Gandin (1963) in an objective analysis technique in order to optimally minimize errors of interpolation. Both structure and correlation functions, which are related when normalized, provide a means of comparing data from unlike instruments which supposedly give the same meteorological measurements. For this reason, both satellite infrared soundings and conventional soundings can be co-analyzed by using these methods. Although results are expected to be dependent on the measuring instrument used and on the extent of the analyzed data sets, this procedure provides a means for statistical comparison and use of the different data sets in optimal interpolation or field matching, as suggested by Gandin.

The structure function for the deviation of a quantity f from its mean is defined as the mean squared difference between values such as temperatures, at two points r_1 and r_2,

$$b(r_1,r_2) = \overline{\left[f'(r_1) - f'(r_2)\right]^2} \tag{1}$$

where

$$f'(r) = f(r) - \overline{f}(r) \tag{2}$$

A closely related function is the correlation (autocorrelation) function defined as the mean product of the deviation of f from its mean at two points, r_1 and r_2.

$$m(r_1,r_2) = \overline{f'(r_1)f\ (r_2)} \tag{3}$$

The relationship between the structure and correlation function can be shown to be

$$b(r_1,r_2) = m(r_1,r_1) + m(r_2,r_2) - 2m(r_1,r_2) \tag{4}$$

where the first two terms are the variances of the deviations of f at points r_1 and r_2 respectively, and the third term is the covariance between deviations at points r_1 and r_2. For the case of homogeneity and isotropy the structure function depends only on ρ where

$$\rho = | \vec{r}_2 - \vec{r}_1 | \tag{5}$$

So, the structure function becomes

$$b(\rho) = 2m(0) - 2m(\rho) \tag{6}$$

where $b(0) = 0$,

$b(\rho)$ increases with ρ, because $m(\rho)$ decreases with ρ, and

$b(\infty) = 2m(0)$, because $m(\infty) = 0$ (no correlation).

2.3 Satellite Soundings and Area of Study

The satellite soundings used in this statistical structure and correlation function analysis were retrieved from satellite radiances recorded by the Vertical Temperature Profile Radiometer (VTPR) on NOAA 4. The VTPR instrument has been launched on all NOAA satellites since 1972.

NOAA polar-orbiting satellites have sun-sunchronous orbits with local 9 am and 9 pm equator crossing times. Operational temperature retrievals from VTPR radiances are not performed over land areas but only over data sparse regions, such as the oceans. However, an iterative method for retrieving temperature profiles over the U.S., for example, from VTPR radiances was developed which uses conventional rawinsonde soundings to create an appropriate initial guess profile. The retrieval procedure used in this study is outlined in Hillger and Vonder Haar (1977).

Rawinsonde soundings create the best initial guess profile when they have close space and time proximity to the satellite radiances. The conventional soundings help determine boundary conditions, such as surface temperature and pressure, which need to be known in any retrieval scheme which uses the radiative transfer equation explicitly. The rawinsonde soundings also more clearly define the tropospheric lapse rate and moisture content. This information is used to initialize the transmittance functions in the retrieval process.

The radiance channels and wavelengths for the VTPR instrument are given in McMillin et al. (1973). The six 15 μm CO_2 channels, with weighting functions shown in Figure2.1 were used actively in the temperature retrieval algorithm. The CO_2 channels respond mainly to atmospheric temperature changes. The window channel at 12 μm senses surface temperature changes primarily, but it was not used in the retrieval process. The H_2O channel at about 19 μm was, on the other hand, used passively to obtain moisture information as a residual in the retrieval process. This method of obtaining moisture information was used successfully in Hillger and Vonder Haar (1976 and 1977).

The area of interest for this study was centered on the National Severe Storm Laboratory (NSSL) mesoscale sounding network shown in Figure 2.2

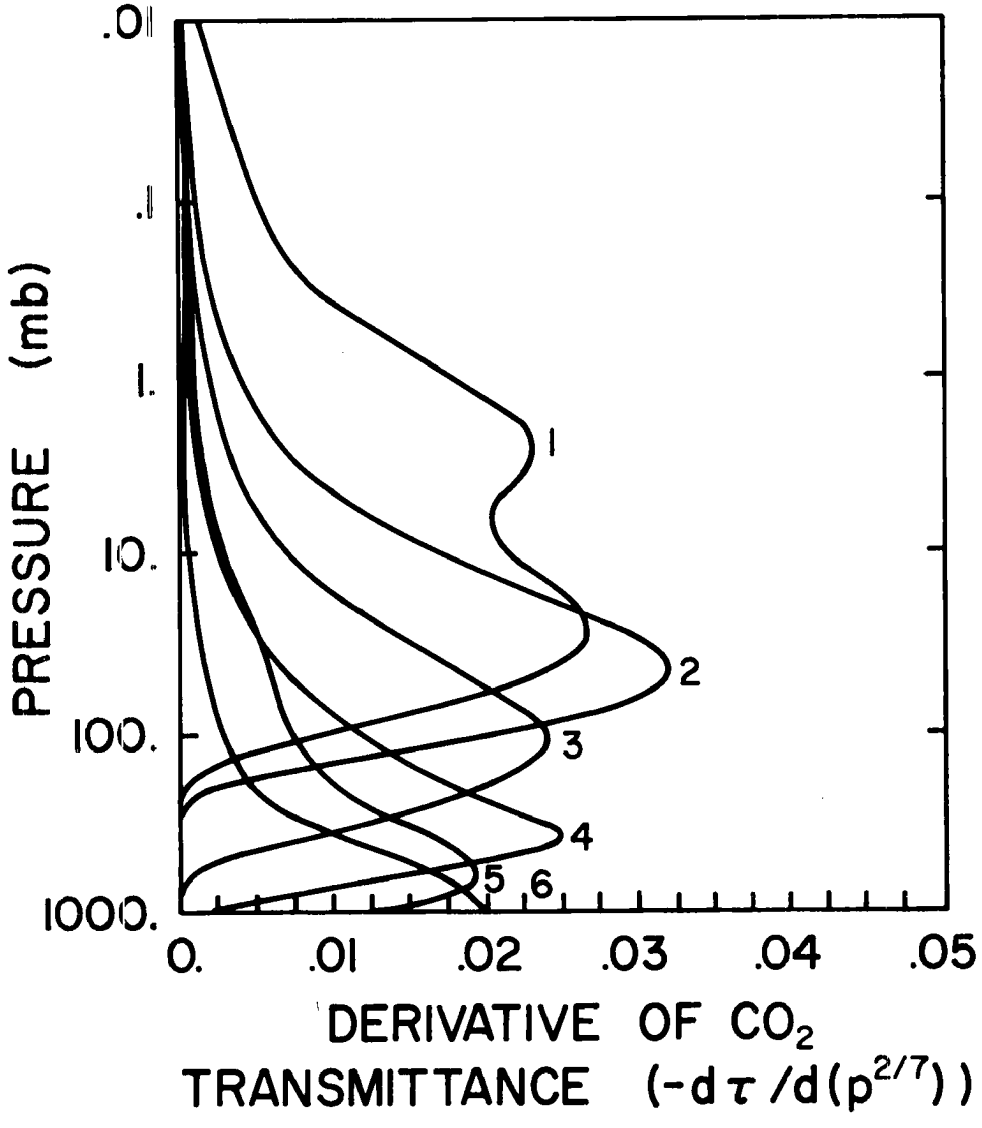

Figure 2.1 VTPR CO_2 Channel Weighting Functions for U.S. Standard Atmosphere.

The nine stations were launch sites for soundings taken at both 0900 CST and 1430 CST. The 0900 CST (1500 GMT) launch time is within one hour of the NOAA satellite descending (daytime) orbit at approximately 1500-1600 GMT at this latitude. The temperatures and mixing ratios from the NSSL rawinsondes were independently analyzed by Barnes using statistical structure and correlations functions, computed as in previous years' analysis of NSSL data (Barnes and Lilly, 1975). The only active use of the NSSL soundings in this study of satellite soundings was to create an initial guess profile for the iterative retrieval algorithm. All nine soundings at 0900 CST were combined to form one mean profile for each NSSL day. This mean temperature and moisture profile was then used as a starting profile in the retrieval of temperatures from the VTPR sounding radiances obtained on that day.

The sub-satellite tracks for the NSSL mesoscale sounding period are shown in Figure 2.3. Of the 32 available days for the NSSL period)10 May - 12 June, 1976) only 14 days proved to have sufficient near-nadir radiances over the NSSL sounding grid. The days that were analyzed were every other day between 76/5/10 and 76/5/22 and between 76/5/29 and 76/6/10 The polar-obtiting NOAA satellites have roughly a two day period where they pass close enough overhead for comparisons to be made. The in-between days have sub-satellite tracks on either side of the area of interest. All possible satellite soundings retrieved within the large 9^{o} latitude by 10^{o} longitude box shown in Figure 2.3 were used for the structure function and correlation function analysis of the satellite soundings.

2.4 Comparison to NSSL Mesoscale Structure Functions

A statistical structure function analysis was performed on the 1976 NSSL mesoscale soundings which were launched at 0900 CST. This analysis

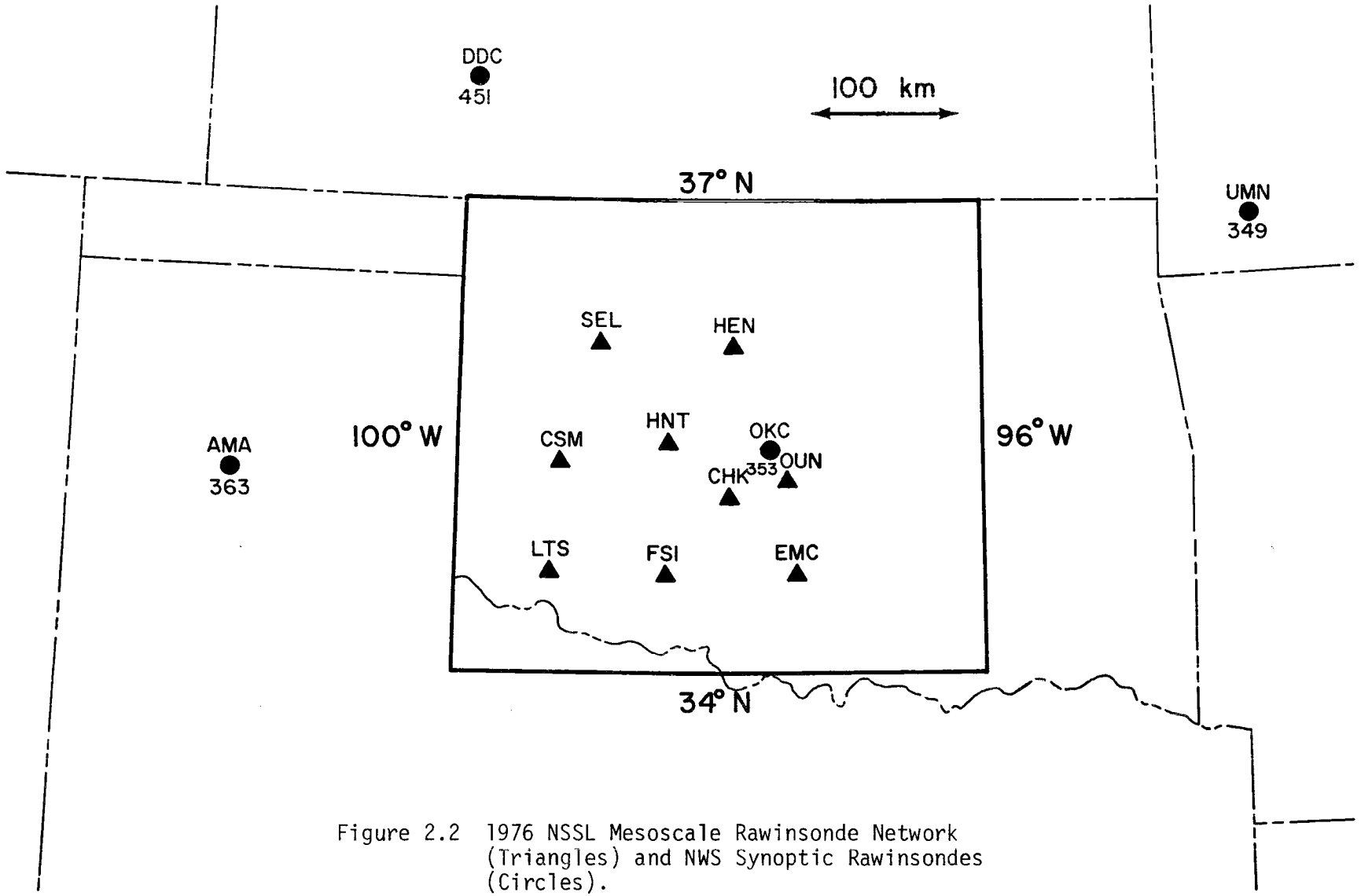

Figure 2.2 1976 NSSL Mesoscale Rawinsonde Network (Triangles) and NWS Synoptic Rawinsondes (Circles).

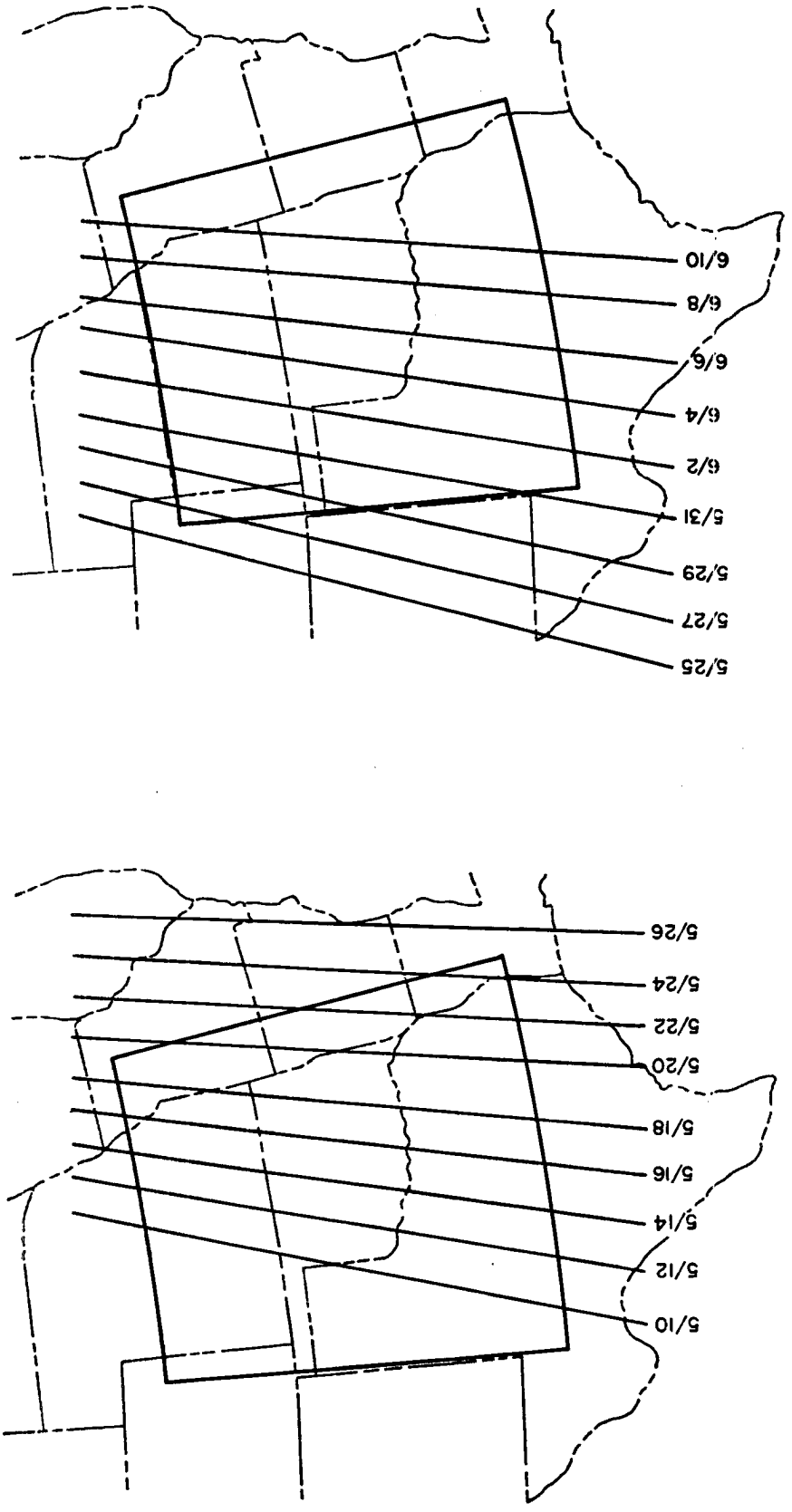

Figure 2.3 Sub-Satellite Tracks for 1976 NSSL Mesoscale Sounding Period (10 May - 12 June 1976).

was performed by Barnes (1977) in a manner similar to that used on NSSL data from 1966 through 1968 (Barnes and Lilly, 1975). The results for layer-averaged temperatures are shown as solid lines in Figure 2.4 and 2.5 for 500 and 700 mb respectively. The lines were fit to data points, one point corresponding to each pair of stations in the network shown in Figure 2.2. The structure functions were also forced to a value of zero at zero separations distance, so no equivalent noise level was derived for the rawinsonde data.

The dashed lines in Figures 2.4 and 2.5 are portions of the structure functions for the satellite data. The smallest separation distance for these curves is at 75 km where the solid and dashed lines intersect. However, at larger distances the structure function values for the satellite temperatures are less than those for the rawinsonde temperatures, this difference is easily explained by the different vertical depths over which the temperatures were averaged. Barnes used a 900 m vertical averaging distance while the satellite temperatures are inherently averaged over a larger vertical depth.

Several papers have dealt with the vertical resolution of satellite soundings including Conrath (1972) and Rodgers (1976). All vertical resolution studies deal with the tradeoff between vertical resolution and noise. Conrath determined an intrinsic vertical resolution of 300 mb or 4500 m at the 500 mb level. The resolution does increase with pressure and decrease with height. However, Thompson et al. (1976) showed that anomalies with characteristic thickness less than the theoretical resolving length can be sensed by VTPR. The resolving length, therefore, corresponds to neither a minimum thickness of anomaly which can be retrieved nor a minimum thickness of physically significant structure in the retrieved profile.

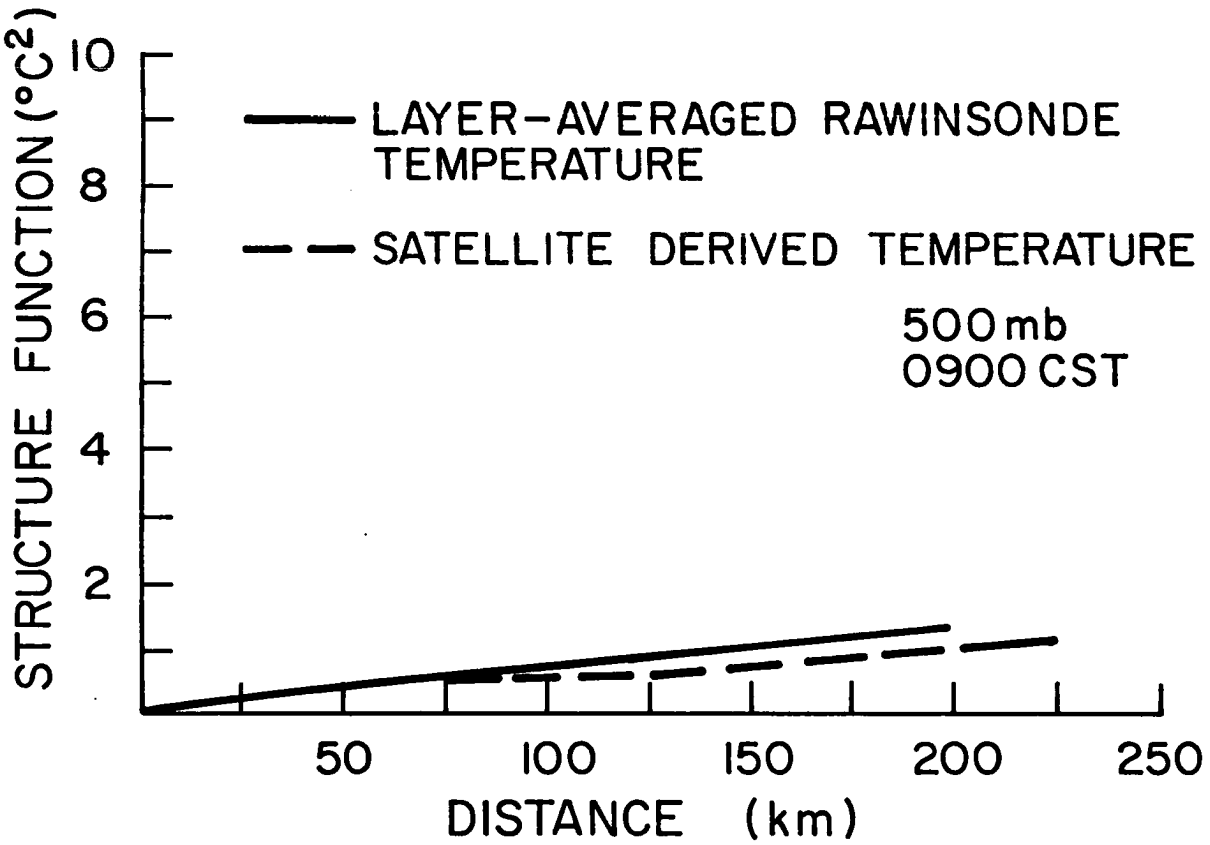

Figure 2.4 Structure Functions for Layer-Averaged Rawinsonde Temperatures and Satellite-Derived Temperatures at 500 mb for all NSSL Sounding Days at 0900 CST.

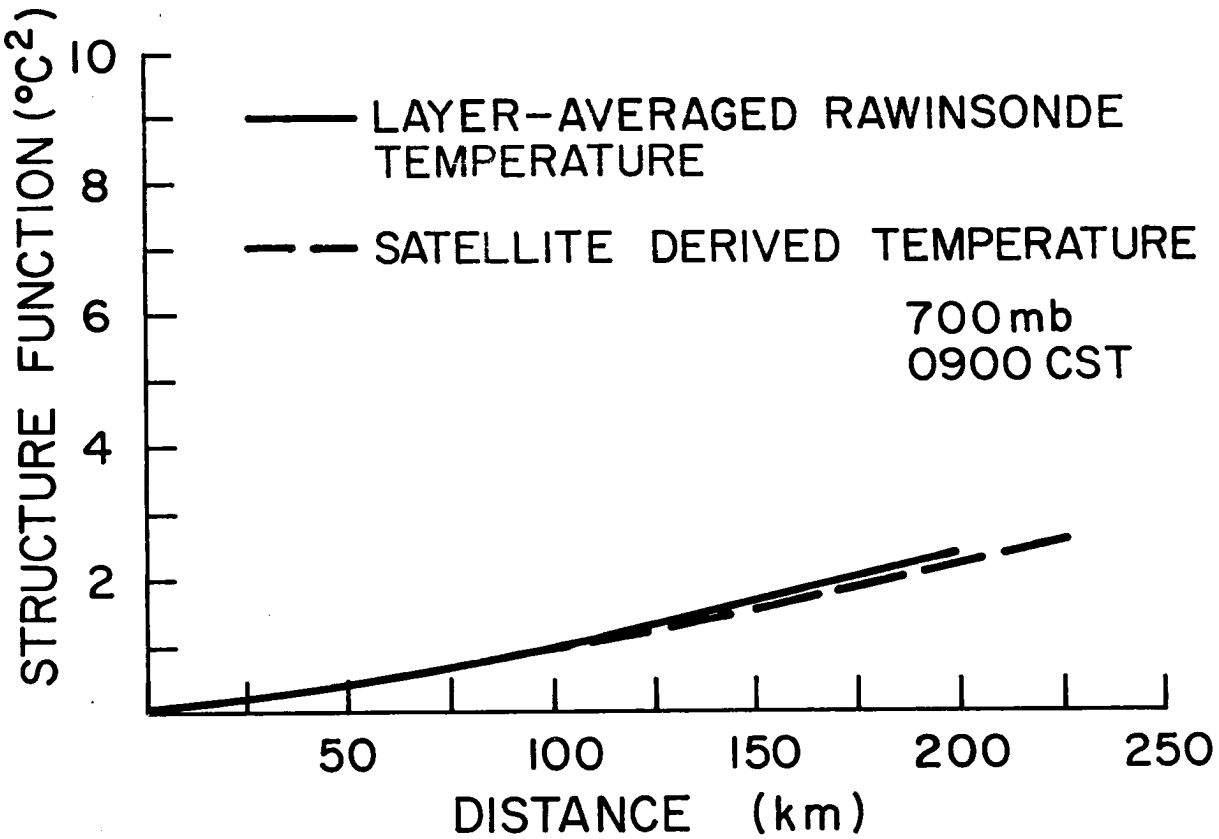

Figure 2.5 Structure Functions for Layer-Averaged Rawinsonde Temperatures and Satellite-Derived Temperatures at 700 mb for all NSSL Sounding Days at 0900 CST.

Figure 2.6 shows the correlation functions for moisture. The solid and dot-dash lines are results for layer-averaged rawinsonde mixing ratios at 700 and 500 mb respectively. The dashed line was derived from the satellite moisture residual. Here the much higher correlations at larger distances are due to the vertically integrating effect of the one moisture value derived from the satellite radiances. This integration reduces the effect of higher order changes which can occur at one or several atmospheric levels. For this same reason, the correlations for the lower-averaged mixing ratio at 700 mb are higher than those for 500 mb. Most atmospheric moisture resides in low tropospheric levels with only occasional mixing to higher levels.

These structure functions and correlation functions for temperature and moisture compare favorably for the two data sets, considering the inherent vertical-averaging differences. Now we will look at the structure function for some individual days to see how this statistical mean gradient can be used to determine significant weather situations.

2.5 Structure Function for Individual Days

This structure function analysis can be applied to each day on an individual basis. The only problem with this approach is that some days may be too cloudy and may not contain a large enough sample of cloud free radiances for statistical analysis. However, if there are enough cloud free columns, then the structure function will give a mean non-directional gradient for that day. This mean gradient of temperature or moisture can tell us if there is a possibility of severe weather events later that day. Large gradients in temperature and moisture usually are precursors to lines of summertime convective activity and subsequent severe weather. These gradients can be determined from conventional data, but

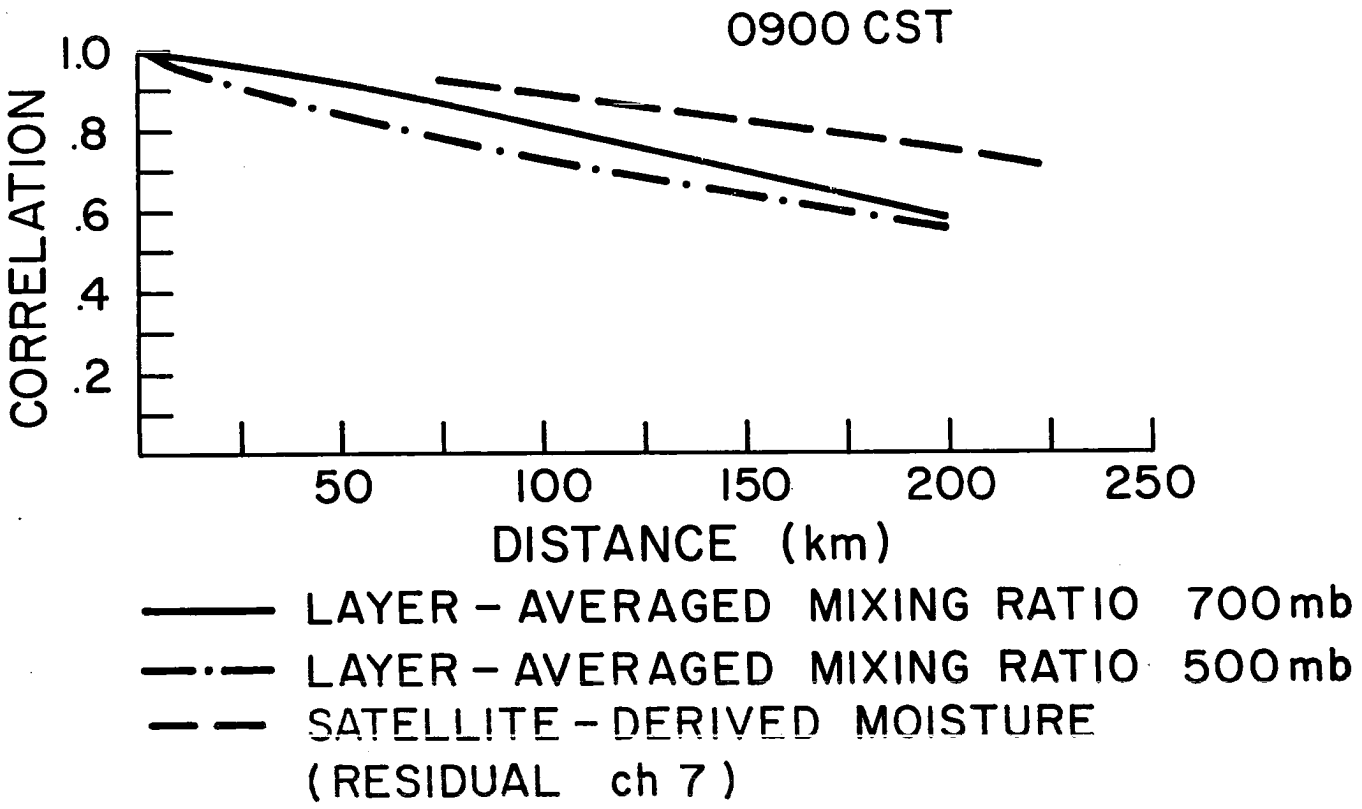

Figure 2.6 Normalized Correlation Functions for Layer-Averaged Mixing Ratios at 500 and 700 mb and Satellited-Derived Moisture for NSSL Sounding Days at 0900 CST.

the satellite radiances are also capable of detecting these gradients without any conventional sounding information.

The structure functions for the scan angle corrected radiances for channel 6, the lowest CO_2 channel, for ten of the fourteen days are plotted in Figure 2.7. Two days were too cloudy to contain a large enough statistical sample, and two other partly cloudy days were not plotted to avoid over-crowding of the figure. The remaining days were either clear or they had structure functions which showed significant change in structure with increasing separation distance.

Table 2.1 lists the significant weather events, if any, for all 14 days on which the structure function analysis was applied. These weather events were gathered from severe weather reports in Oklahoma and northern Texas, the area for which the radiances were obtained. About half the days had no significant weather activity. The remaining days either reported thunderstorms or hail. Two days in particular, 76/5/29 and 76/5/31, had reports of both funnel clouds and hail. These two days also have the largest structure function increases with distance shown in Figure 2.7 up to a separation of 500 km and beyond. Since the VTPR channel 6 radiance mainly responds to temperature changes in the lower troposphere, these large changes reflect large lower-tropospheric temperature gradients. On the other hand, the days with no significant weather activity show the smallest structure functions. For example, 76/5/18, which was clear, had the lowest structure values at almost all separation distances. On this day there was little change in observed temperature across the field as sensed by the VTPR radiance for channel 6.

Figure 2.8 shows the structure functions for the same 10 days, but for the radiances from VTPR channel 7. Channel 7 is affected mainly by

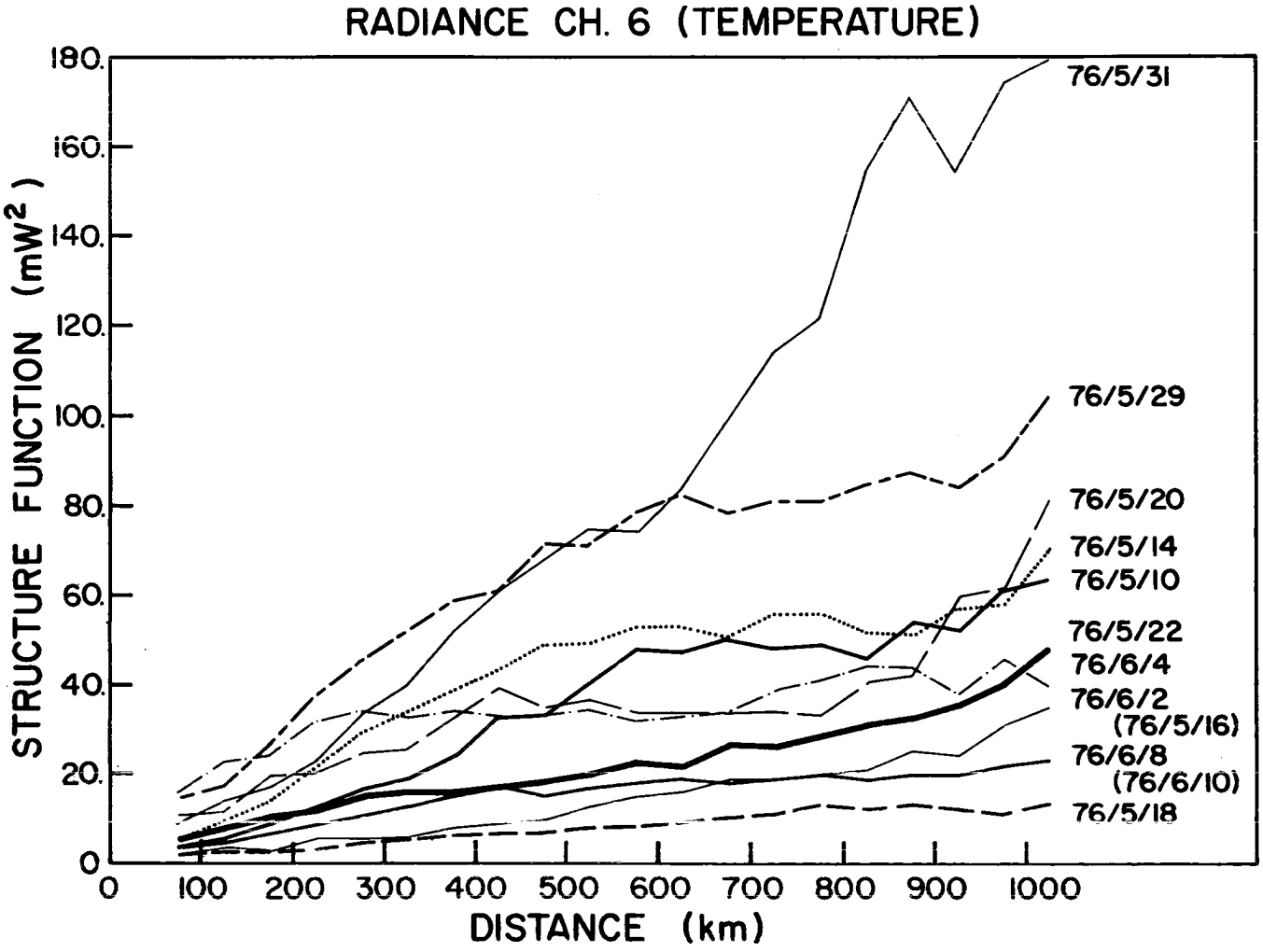

Figure 2.7 Structure Functions for VTPR CO_2 Channel 6 on Individual NSSL Sounding Days.

Table 2.1

Date	Number of Pairs: Radiances	Number of Pairs: Temperature	Qualitative Cld Cover at approx. 1600 GMT	Significant Weather: Event	Significant Weather: Time (GMT)*
76/5/10	8094	3154	2	hail	0600-0700
76/5/12	489	12	4 (cloudy)	hail	1715-0040
76/5/14	7194	6375	2	No activity	
76/5/16	4276	2626	3	No activity	
76/5/18	13130	12969	1 (clear)	No activity	
76/5/20	7074	2140	3	thunderstorms°	
76/5/22	7578	1081	3	hail	0105-0335
76/5/29	8230	2343	2	funnel clouds -hail	2300-0300
76/5/31	3870	1952	3	funnel clouds -hail	2200-0200
76/6/2	12966	7004	1 (clear)	thunderstorms°	
76/6/4	9110	2742	2	thunderstorms°	
76/6/6	5298	723	4 (cloudy)	thunderstorms°	
76/6/8	11852	4521	2	No Activity	
76/6/10	11124	6055	2	No Activity	

\+ Qualitative cloud cover from window channel radiances
(1=mostly clear, 4= mostly cloudy)

* from Storm Data reports (May-June 1976)

° from 2345 GMT SMS visible images or NOAA SR images

moisture changes and to a lesser extent by temperature changes. The same two days, 76/5/29 and 76/5/31, again show large structure function increases with distance. However, three other days also show large changes, 76/5/20, 76/6/4, and 76/6/8. Two of these three days reported thunderstorm activity but no other severe weather. These gradients in moisture are important to severe weather development, but they must be coupled with a large temperature gradient as reflected by the structure for VTPR channel 7. The remaining days had lower structure values, and the clear, no activity day, 76/5/18, again had nearly the lowest structure values.

To see how these mean radiance gradients propagate into the derived temperature gradients, the structure functions for 500 mb temperatures are shown in Figure 2.9. The days 76/5/29 and 76/5/31 still maintain large temperature gradients at 500 mb. This may signify a cold trough in the upper atmosphere. Other days had structure function values with magnitudes equal to the structure on 5/29/76, up to 600 km. The structure functions for 500 mb temperatures, however, do not show as great a distinction between severe and non-severe days as do the radiances for channels 6 and 7. Upper air support does have an effect on summertime convective activity, but the most important ingredients are lower troposphere temperature and moisture gradients.

Table 2.1 also lists the number of pairs of radiances and temperatures which went into the structure function analysis for each day. The high variability of the structure functions on some days was due to the small number of pairs in some of the 50 km intervals. The cloud cover index (from 1 to 4) in Table 2.1 also shows which days were mostly clear (1) or mostly cloudy (4). The clearest days, for example 76/5/18 and 76/6/2, have the smoothest structure functions, and cloudy days have more variability

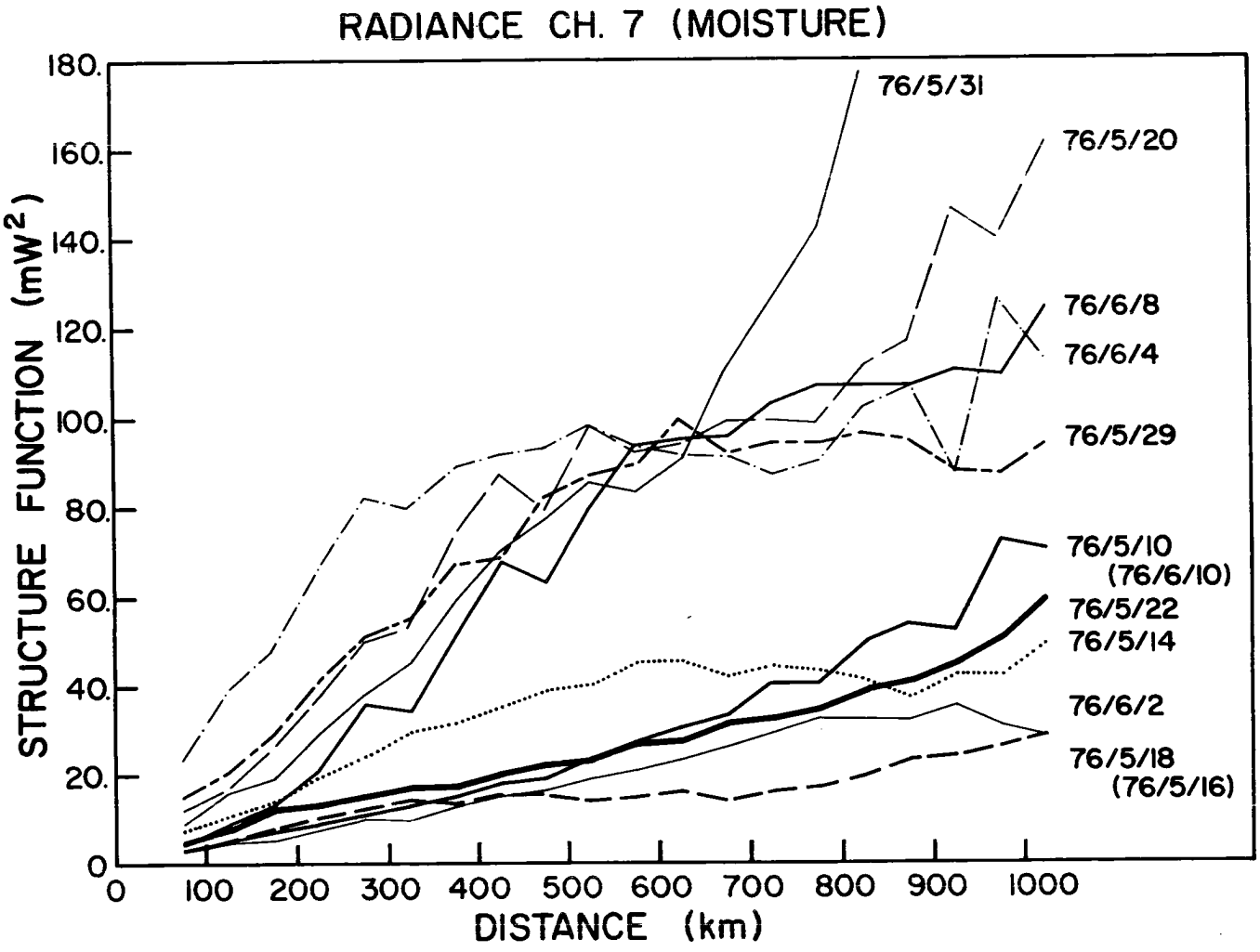

Figure 2.8 Structure Functions for VTPR H_2O Channel 7 on Individual NSSL Sounding Days.

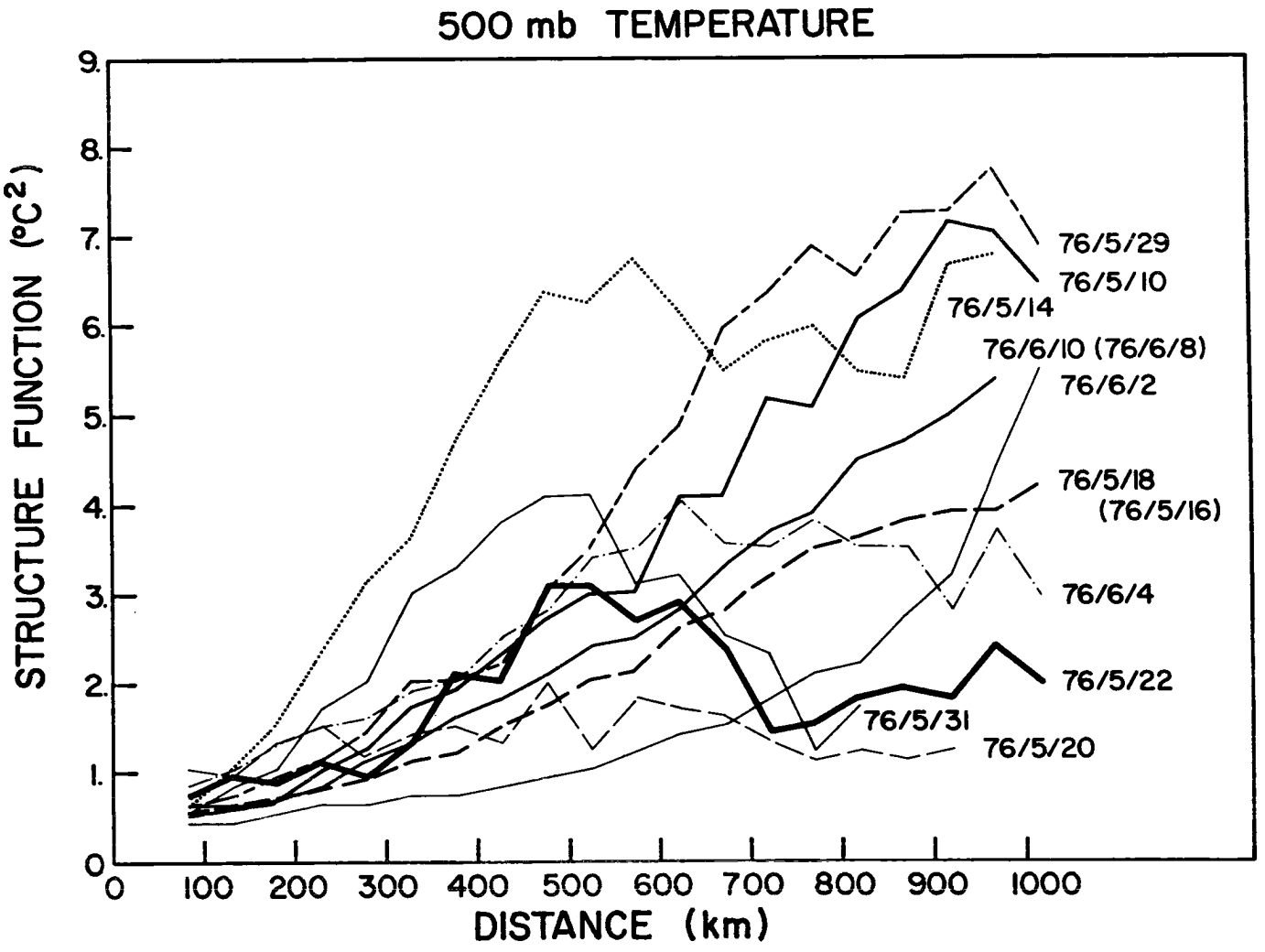

Figure 2.9 Structure Function for Satellite-Derived 500 mb Temperatures on Individual NSSL Sounding Days.

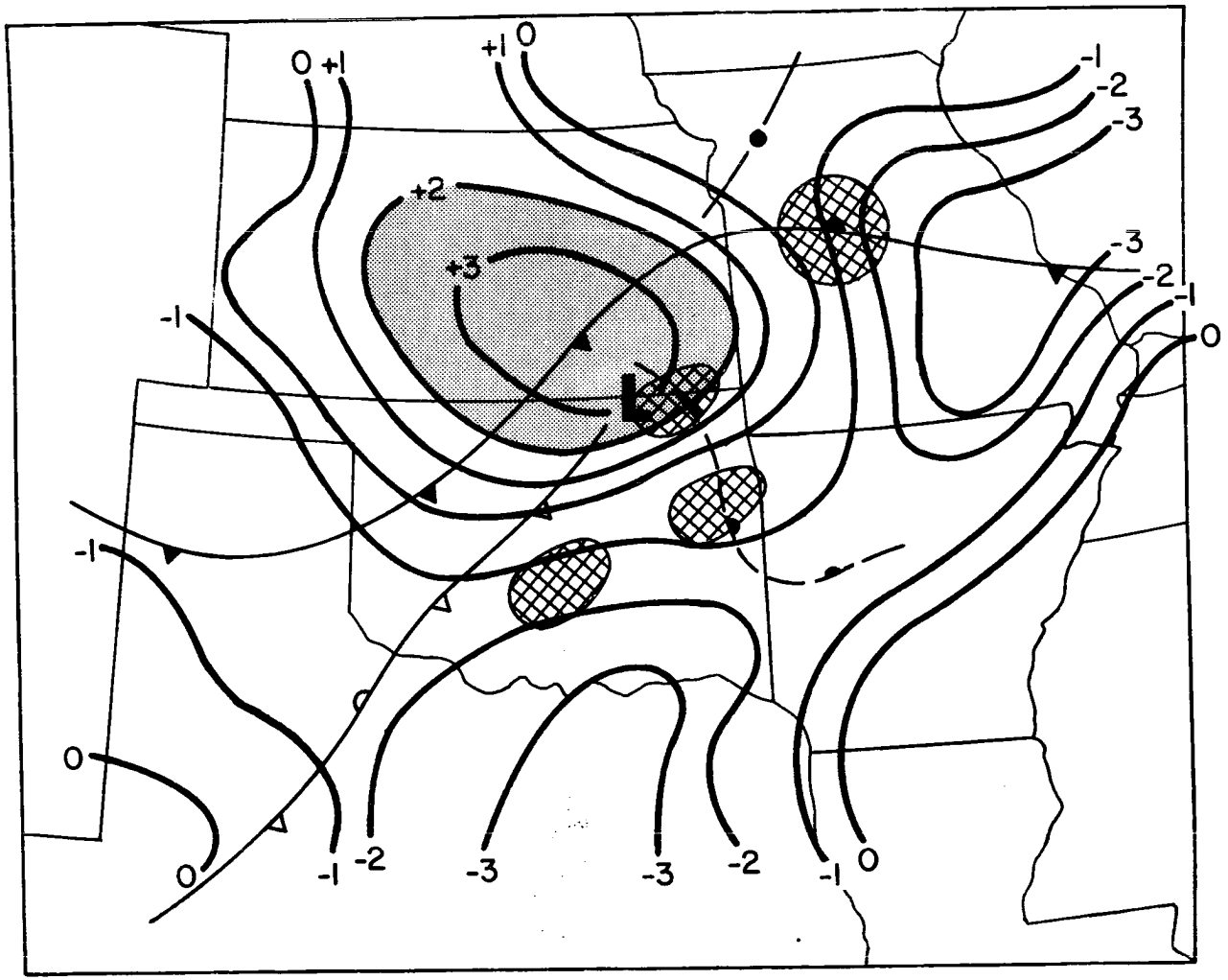

Figure 3.1 700 mb vertical velocity in μbars s^{-1} (from Wilson, 1976). Regions where severe thunderstorms developed are cross-hatched.

nature of the dominate forcing mechanisms was then investigated. In the pre-storm environment, low-level wind fields from satellite derived cumulus velocities were coupled with surface mixing ratios to derive horizontal moisture fluxes. Magnitudes of such moisture convergence were compared to subsequent storm severity. Continued remote sensing of the cloud field in its growth phase was then accomplished through the use of satellite infrared emitted (IR) blackbody temperature measurements. Rates of growth for several storms of differing severity were examined in an attempt to develop criteria for a short-term prediction-warning scheme. Fujita (1973) has shown that the height of cloud-tops can undergo fluctuations indicative of the changes in the intensity of updrafts within the storm. A final section on the comparison of satellite and radar data details some particular problems in infrared remote sensing, specifically the detection of small intense echos and overshooting domes, and the determination of cloud height for storms penetrating the tropopause.

Figure 3.2 summarizes severe storms reports from Storm Data* on 24-25 April 1975. Significant reports included hailstones of 2.75" (7.0 cm) diameter at Wewoka, Oklahoma at 2315 and a destructive, killer tornado at Neosho, Missouri at 0040 GMT.

3.2 Mesoscale Winds and Moisture

Five minute interval SMS visible channel data of ~1 km resolution were used to derive low-level (cloud-base) wind fields by tracking small cumulus clouds. Winds were tracked on NASA's Atmospheric and Oceanographic Information Processing System (AOIPS). A complete description of the AOIPS and cloud tracking techniques is given by Billingsley (1976). Figure 3.3 is one

---

*A monthly publication of the Environmental Data Service of NOAA.

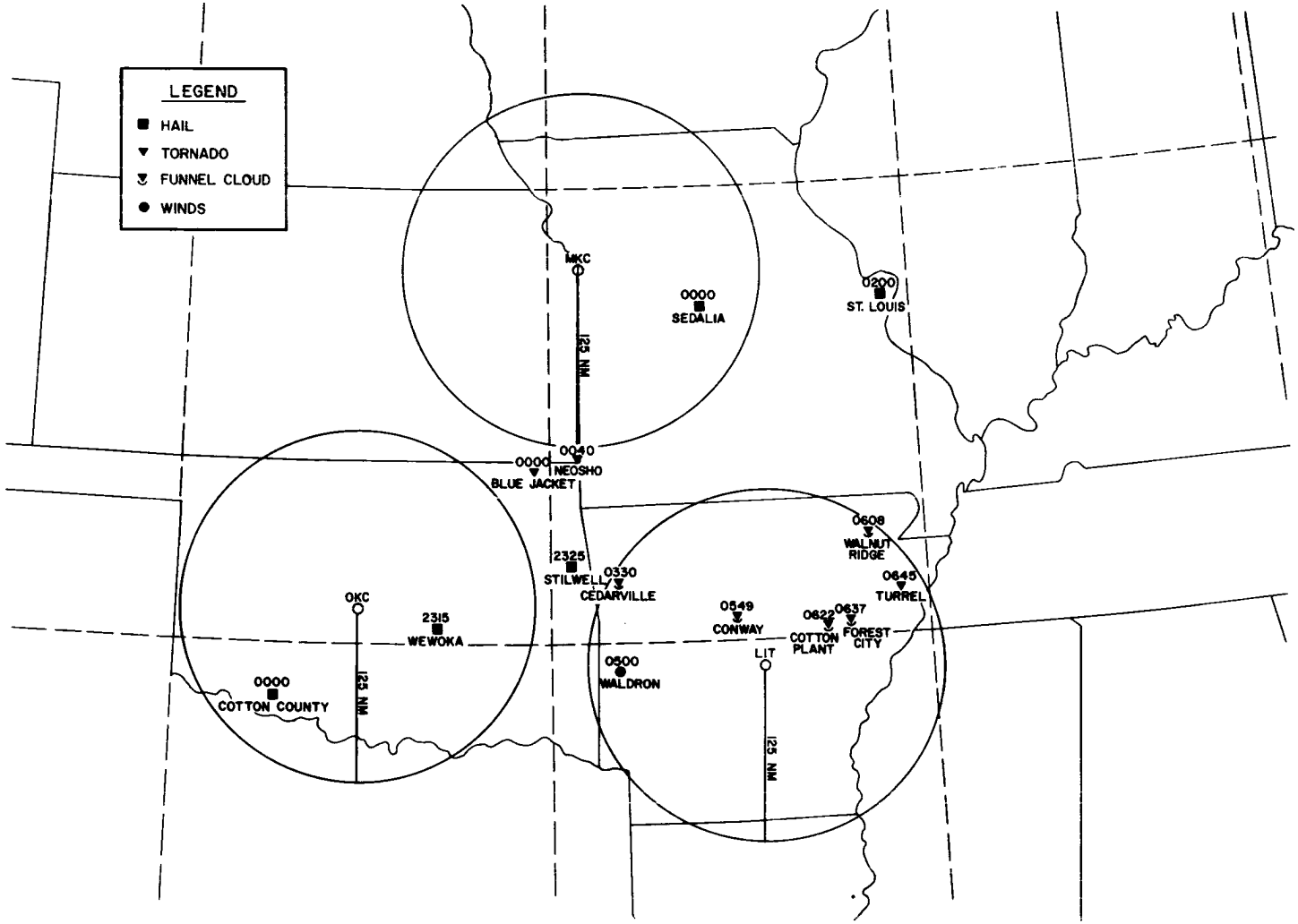

Figure 3.2 Severe storm reports 24-25 April 1975.

satellite visible image used in the sequencing procedure. Clouds were tracked in an area approximately 9^{o} on a side centered near Monett, MO. Intense convective development occurred 1-2 hours after the tracking time. Several complete wind sets were tracked on the AOIPS. Figure 3.4 is a graphical representation of one such set. Lengths are scaled such that a vector of length one degree lat/long represents a wind speed of 17.8 ms^{-1} u velocity and 22.2 ms^{-1} v velocity. Particular problems with cloud tracking include obscuration of low level cumuli by alto-cumulus and cirrus, lack of clouds behind dry lines, and propagation of cumulus along gravity waves. That cumulus motion represents mean winds in the subcloud layer has been demonstrated by Fujita et al., (1975), Hasler et al., (1975) and Suchman and Martin (1976).

The wind field of figure 3.4 was objectively analyzed using a cubic-spline technique. These winds were then combined with 2100 GMT surface mixing ratios (q) and the quantity $\nabla \cdot (qV)$ or moisture divergence was calculated. The resultant field is portrayed in figure 3.5. Units are $g\ kg^{-1}s^{-1} \times 10^{-5}$. All of the severe storms developed within areas of moisture convergence (negative values in figure 3.5). Maximum values of moisture convergence ($\sim 1.7 \times 10^{-3}$ g kg^{-1} s^{-1}) are similar to values found by Sasaki (1973, 1975) to be associated with severe thunderstorm occurrences and tornadic storm development. Similar calculations using 2100 GMT surface winds indicated that an improved correspondence between computed moisture convergence and subsequent severe storm genesis characterized the satellite wind field. With the launch of an atmospheric sounder on a geosynchronous satellite in the 1980's, horizontal moisture flux information may be obtained from satellite sensors alone.

Figure 3.3 SMS-2 visible channel image at 2058 GMT.

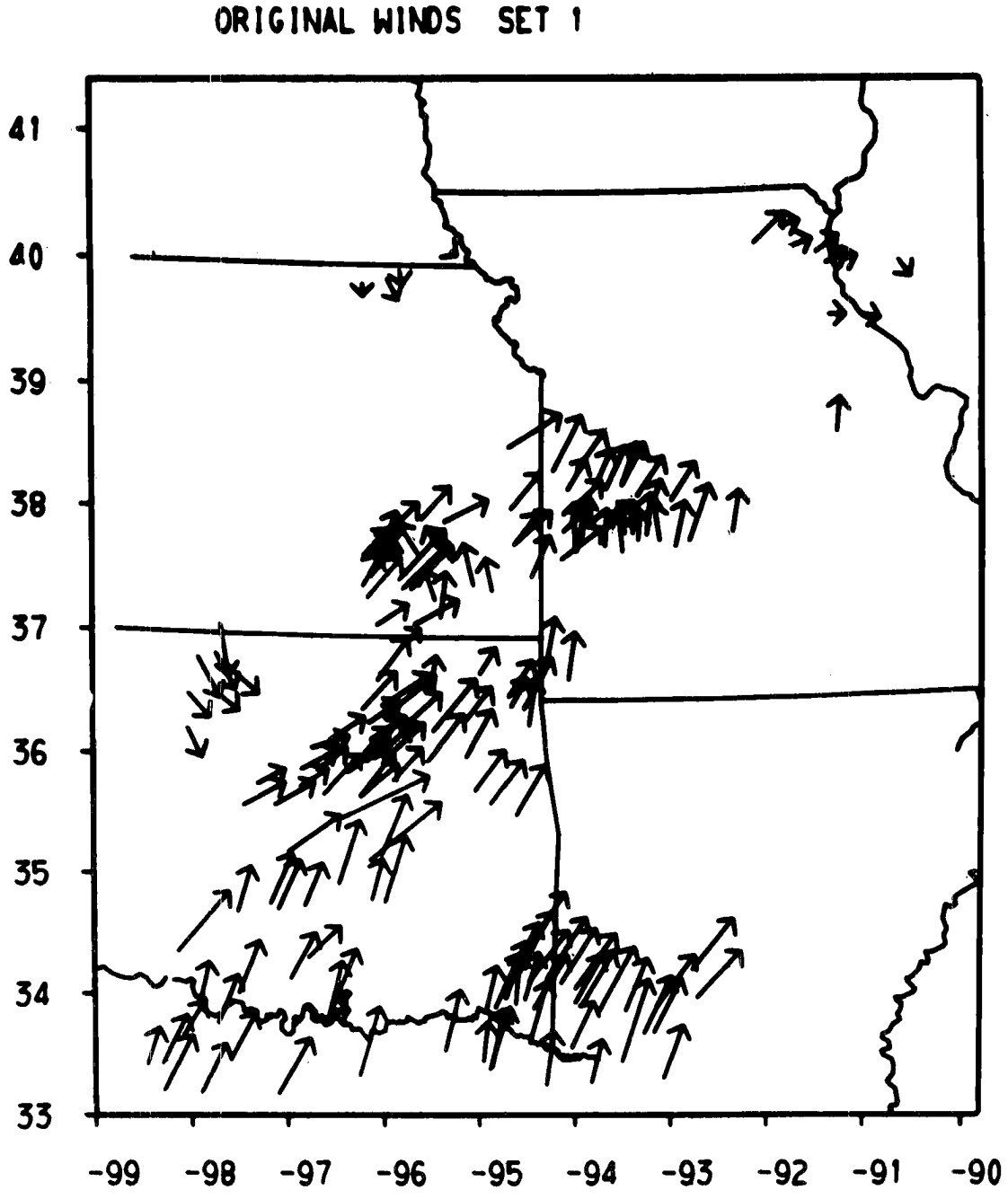

Figure 3.4 Satellite derived wind field at 2100 GMT.

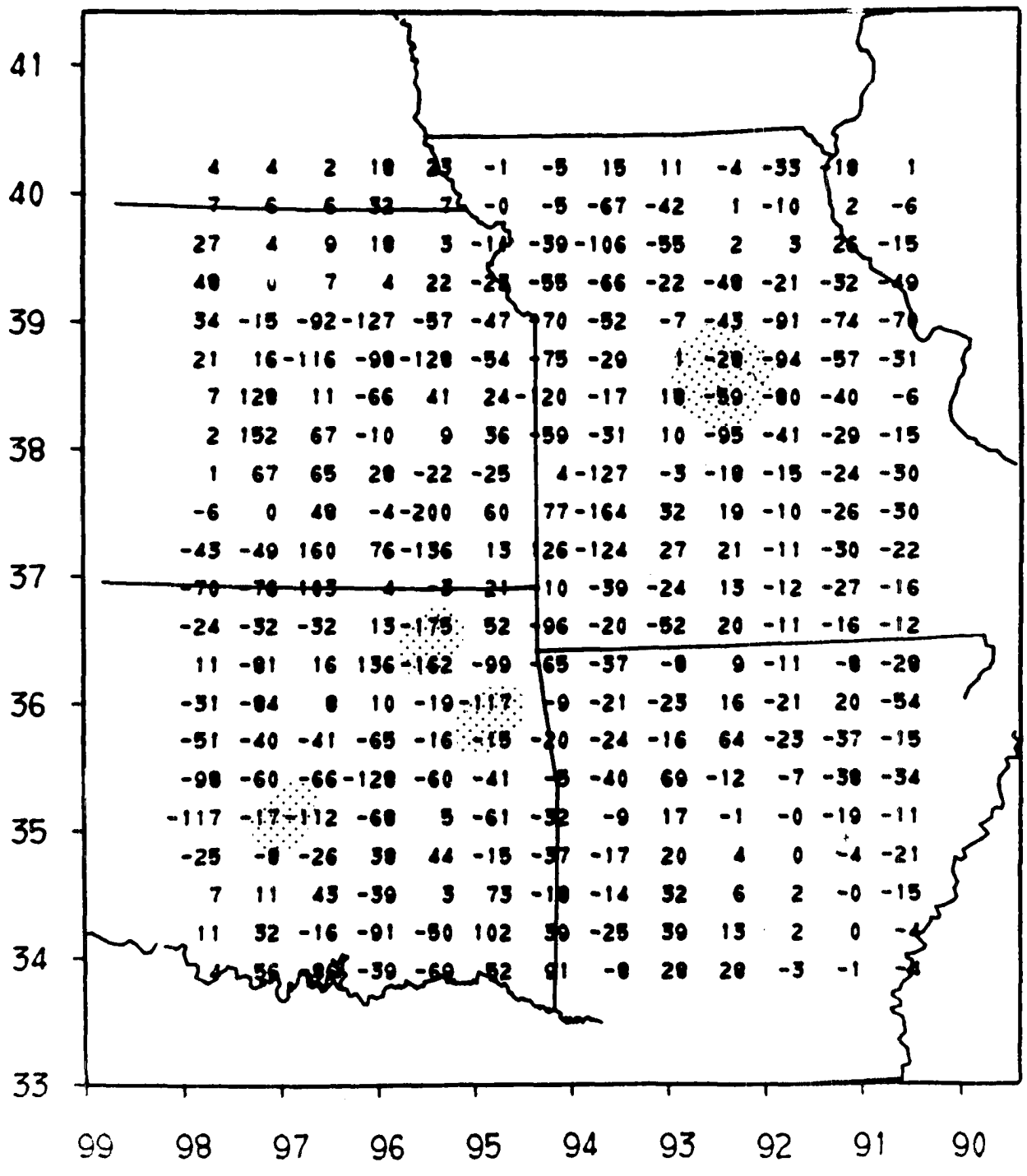

Figure 3.5 2100 GMT moisture divergence from satellite derived winds and surface mixing ratios. Units are g kg^{-1} s^{-1} x 10^{-5}. Negative values indicate moisture convergence. Regions where severe storms developed are stipled.

3.3 Satellite Infrared Growth Rates

Continued observation of thunderstorms in their growth phase by a satellite with high temporal frequency is equally as important as monitoring the pre-storm environment. Satellite measurements in the atmospheric "window" (10-12 μm) can discriminate among convective elements of differing duration and intensity. The intensity of the convection may then help one deduce the severity of the storm. Purdom (1976), and Scofield and Oliver (1977) have presented schemes that deduce tornadic storms and estimate convective rainfall, respectively.

Figure 3.6 is the SMS infrared image at 2242 GMT. Clouds designated by names or numbers become severe storms, while non-severe storm clouds are lettered. Following techniques developed by Adler and Fenn (1976, 1977), infrared growth rates were constructed for these clouds. Starting at the cold end of the temperature spectrum, a cumulative histogram of data points at or below a given temperature are compiled. Thus, a profile of the number of data points N_i, with blackbody temperature $T_{BB} \leq T_i$ is obtained. Adler and Fenn have documented reports of severe weather occurring during, or just after, rapid expansions of cold areas. Results for two severe storms are presented in figures 3.7 and 3.8. Since the ordinate of the graph is logarithmic, the slope of the curves is proportional to the divergence $1/N\ dN/dt$. For example, in figure 3.7, the 222K isotherm which enclosed 7 pixels (~630 km^2) at 2240 expanded to 21 pixels (~ 1890 km^2) in just 5 minutes. In figure 3.8, growth rates for the Wewoka hail storm, divergence values of $1.0 - 5.0 \times 10^{-3}\ s^{-1}$ were found in the pre-hail period, with much slower rates observed after the

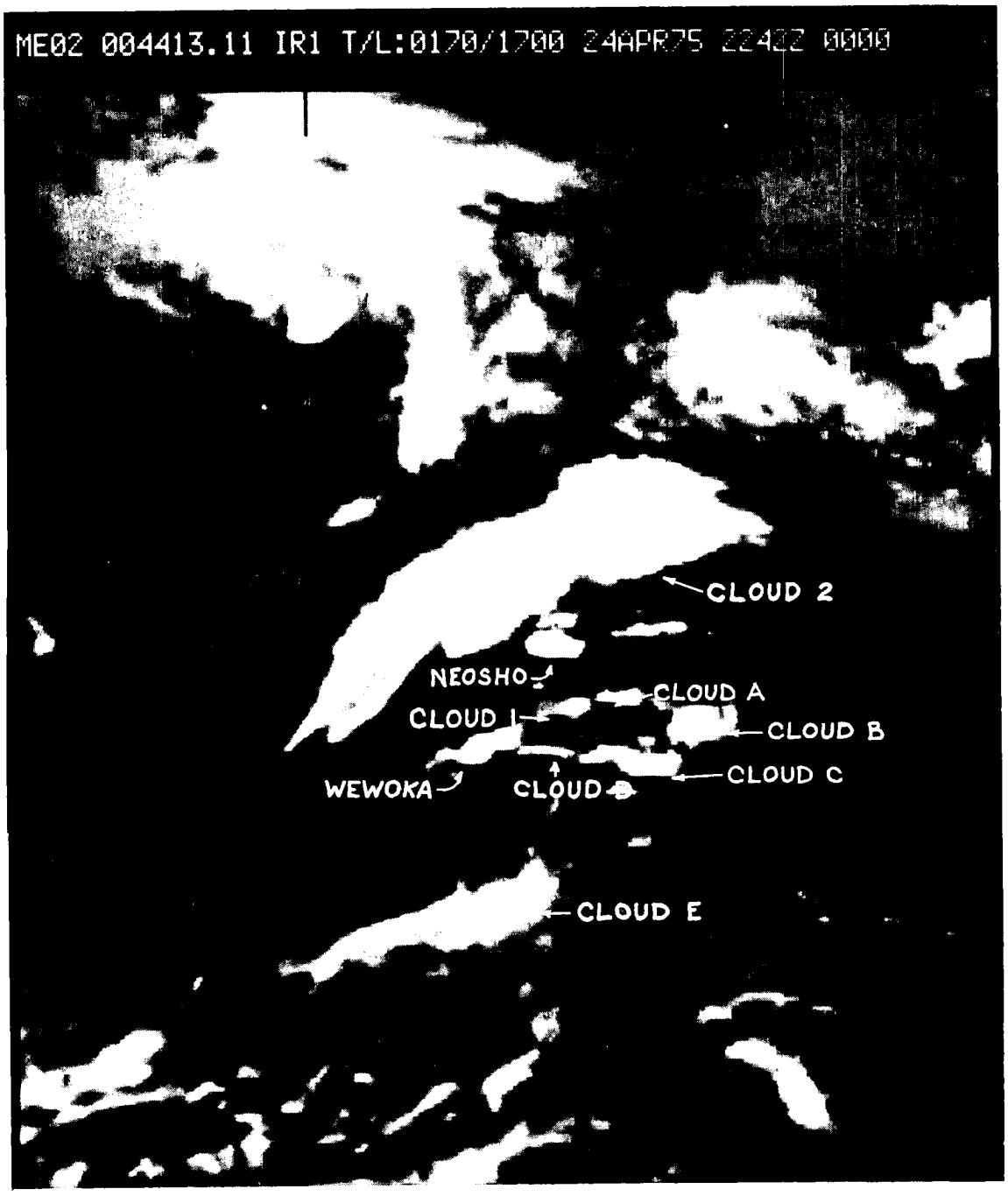

Figure 3.6 SMS-2 infrared image at 2242 GMT. Clouds examined in this study are labelled

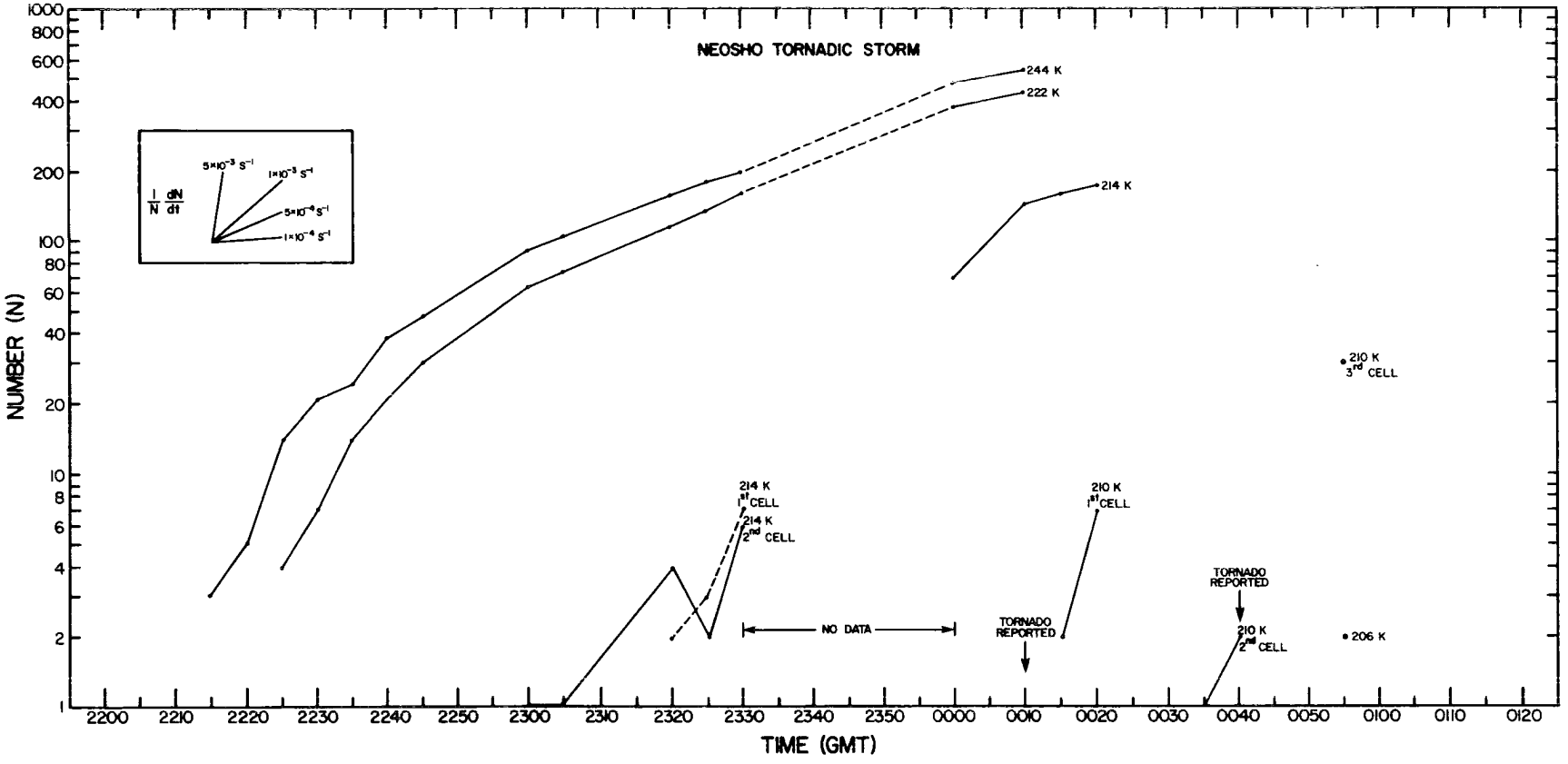

Figure 3.7 Thunderstorm growth rates for the Neosho tornadic storm.

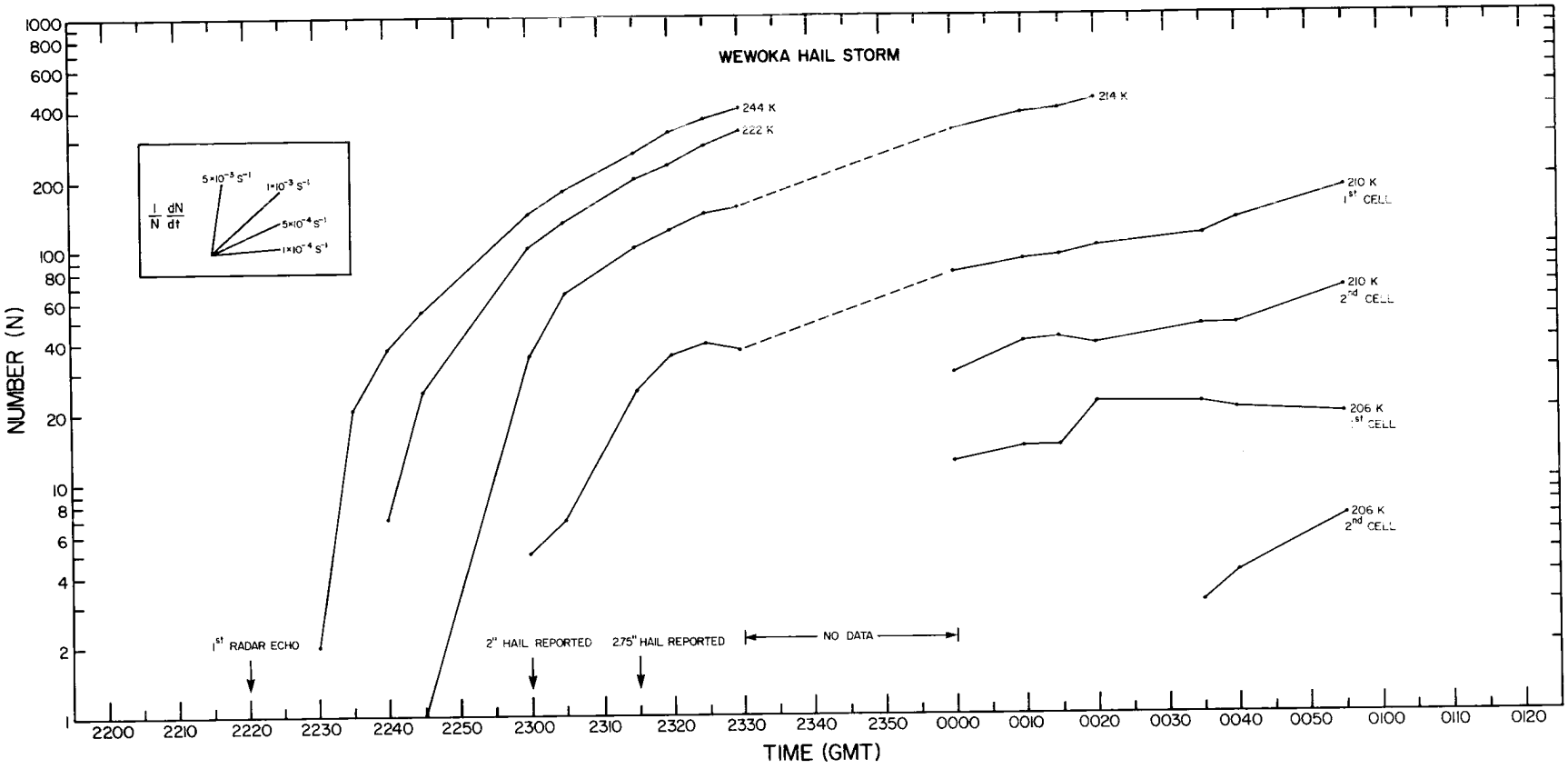

Figure 3.8 Thunderstorm growth rates for the Wewoka hail storm.

occurrence of hail. Growth rates for clouds forming coincidentally with the Neosho and Wewoka storms but which did not become severe are portrayed in figure 3.9. These growth rates rarely exceed $1x10^{-3}$ s^{-1}, and are of shorter duration. While more cases need to be examined, it appears that infrared growth rates are indicative of storm severity, and could be used in a real-time situation to forecast severe weather. Other parameters determinable from satellites that can serve as criteria in a severe - non-severe decision include:

1) relative cloud-top temperature
2) rate of change of minimum blackbody temperature
3) cloud duration and size

3.4 Satellite-Radar Comparison

Intensity contoured radar reflectivities were available for the Wewoka hail storm. In figure 3.10 the temporal variation of echo locations with respect to the fixed location of OKC (dark X's) is shown. The corresponding sequence of infrared images as seen by the satellite is illustrated in figure 3.11. The entire radar echo corresponds to only a small portion of the infrared cloud area. Overshooting domes are not observed in the infrared data due to the coarser resolution and finite response time of the IR sensor (Negri et al., 1976).

For a comparison of storm-top heights, NWS radar summaries were compared to nearly simultaneous heights derived from minimum blackbody temperatures and the Monett, MO environmental sounding. Results are presented in figure 3 12. Below the tropopause, there is fair agreement between heights determined by the two methods of sensing. For storms growing above the tropopause, determination of maximum cloud height from

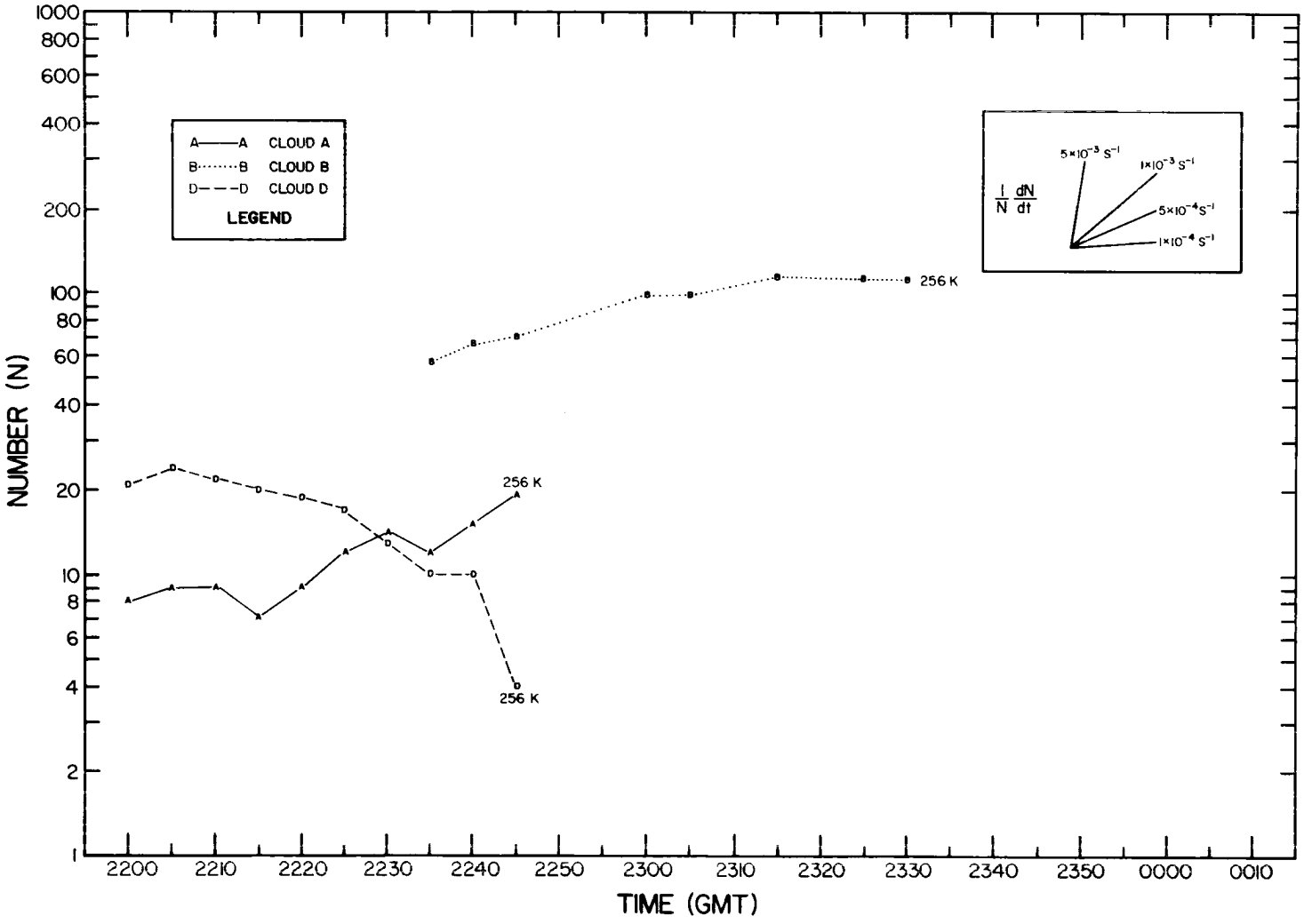

Figure 3.9 Thunderstorm growth rates for several non-severe storms.

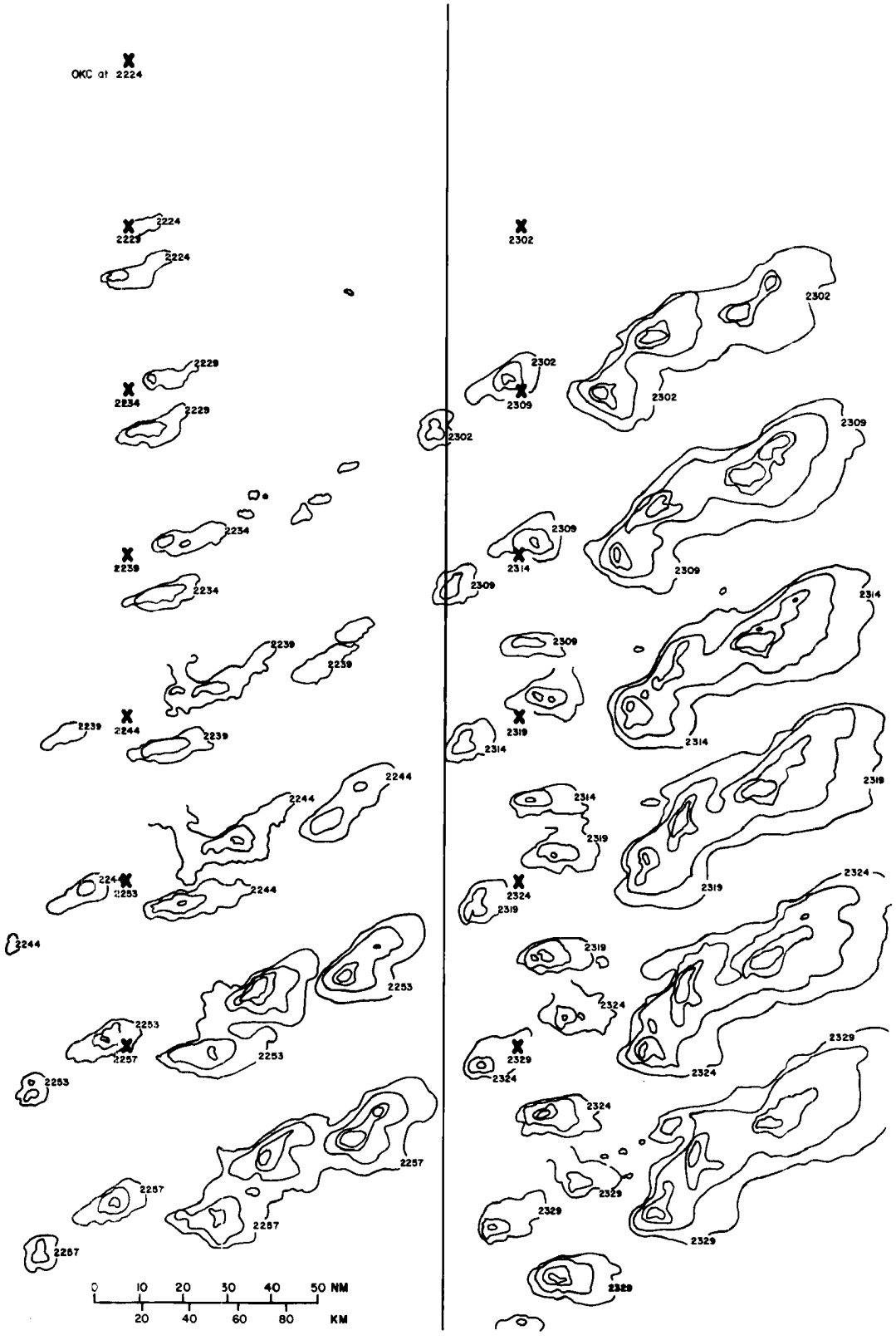

Figure 3.10 Intensity contoured radar reflectivities for the Wewoka storm.

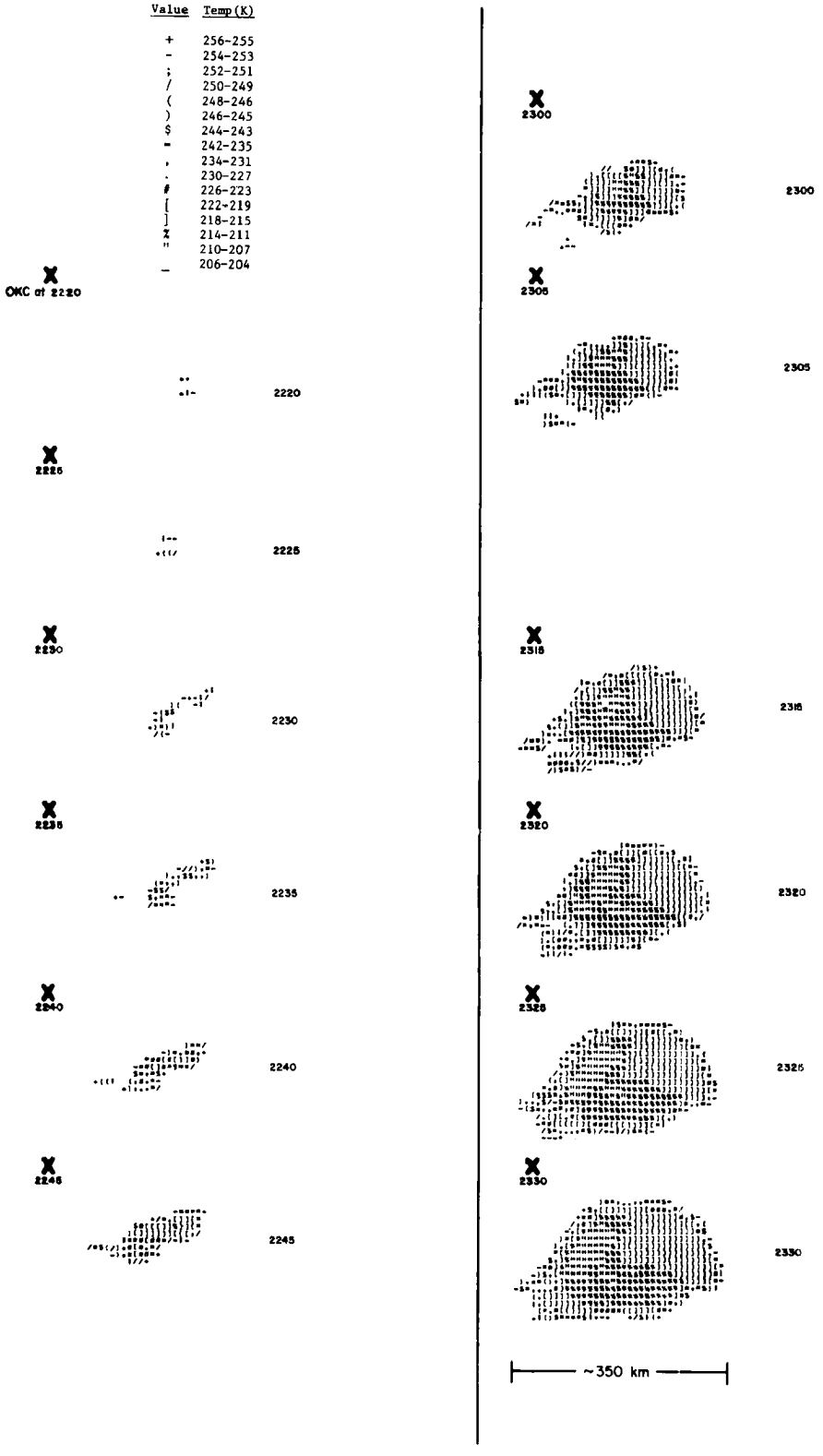

Figure 3.11 Character display of the infrared growth rate of the Wewoka storm.

I_R data alone was not possible. Several factors that may account for the scatter in figure 3.12 are:

1) "inexactness" of reported heights on NWS radar summaries which represent an instantaneous height measurement not well specified in time.

2) infrared resolution of overshooting domes. These domes will have cross-sectional areas of ~ 80 km^2 which is insufficient to fill the field of view (FOV) of the IR sensor.

3) isothermal lapse rate above the tropopause. Overshooting turrets, while cooling moist adiabatically are entraining stratospheric air whose temperature varies little with height. The net effect is to "smooth out" the presence of the overshooting top as viewed by the IR sensor.

4) The finite response time of the IR sensor. Three to four FOV's of the same temperature are required in order to exceed the response time of 55×10^{-5} s. Overshooting domes rarely provide this area.

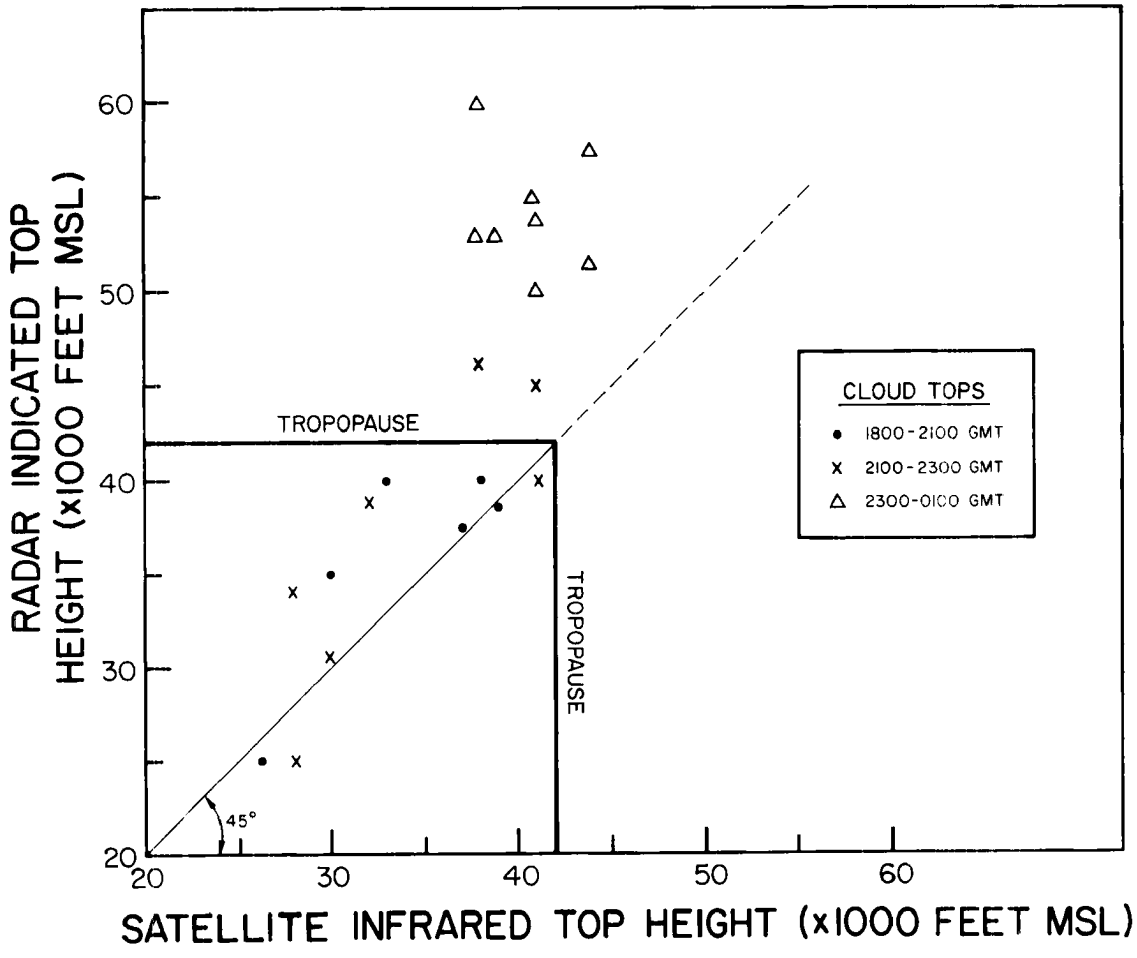

Figure 3.12 Comparison of radar and satellite indicated cloud tops.

4.0 Statistical Structure of Satellite Derived Wind Fields

During the first year of work on grant ATM 76-21307 an initial effort was also made to evaluate the statistical structure of satellite derived low-level wind fields. These winds were obtained by tracking low clouds (cumulus of little vertical development assumed to be located at about the 850 mb level) through a four frame, animated film loop. The images were separated by only five minutes and were obtained prior to the development of several severe thunderstorms--one of which produced a destructive tornado at Neosho, Missouri, (see Section 3.0). The actual tracking was done on the NASA Atmospheric and Oceanographic Information Processing System (AOIPS) at Goddard Space Flight Center, Maryland. One of the two wind sets obtained is shown in Figure 4.1. Correlation and structure functions were computed for this data set using function definitions developed for a single field of satellite data.

Several types of potentially useful information may be determined from the analysis of these functions:

1. An indication of the magnitude of noise due to data measurement and processing systems.
2. Determination of important scales of motion in the data field being analyzed.
3. Determination of relevant grid meshes upon which the data might be objectively analyzed, and perhaps the eventual development of a new mesoscale objective analysis technique.

Knowledge of the climatological spatial correlation functions of meteorological variables has been used in several large, or synoptic, scale objective data analysis schemes that incorporate optimal interpolation techniques following Gandin (1963). Examples and discussions

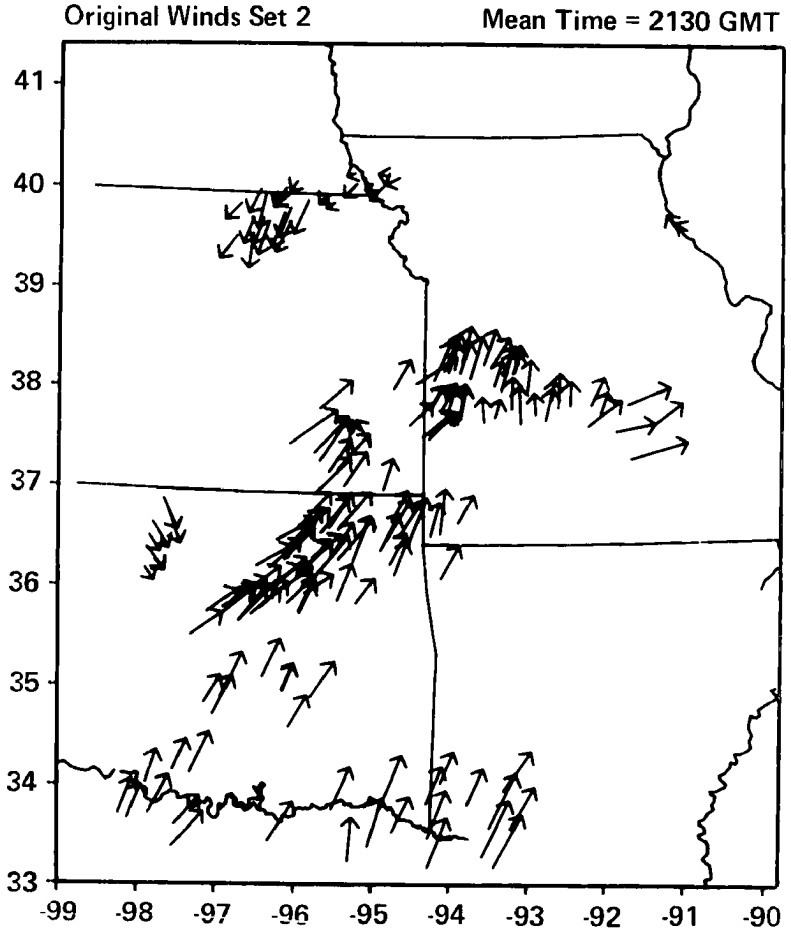

Figure 4.1 Satellite derived low-level wind field for 2130 GMT on 24 April 1975 (200+ vectors).

of some of these techniques may be found in Otte-Bliesner, et al. (1976), Schlatter (1975), and Thiebaux (1975). Barnes and Lilly (1975) presented results of a mesoscale study of the variability of meteorological parameters that indicated a significant fraction of the total variance of the wind and moisture fields occurred at scales of 200 km or less.

During the course of the work reported here the following definitions were developed:

1. Structure function, b,

$$b(R) = \sum_{1}^{N} [f^1(r_i) - f^1(r_j)]^2/N$$

where R is a given distance interval, such as $10 \text{ km} \leq R \leq 20 \text{ km}$. N is the number of data pairs r_i, r_j whose separation distance is within interval R, and $f^1(r_i) = f(r_i) - \bar{f}$ where $\bar{f} \equiv$ the spatial mean of the data set.

2. Correlation function, μ,

$$\mu(R) = \sum_{1}^{N} | f^1(r_i) * f^1(r_j)|/N*m$$

where $m \equiv$ the spatial variance.

These definitions are substantially different then those of Gandin (1963) which employ climatological means of the variable measured within a fixed network of observing sites. All of the ramifications of these modifications have yet to be determined; however, an advantage gained in using satellite data and these definitions is that, since each data point interacts with each other data point, a very large sample size is immediately obtained.

The correlation and structure functions are shown in Figure 4.2 for the wind set of Figure 4.1. Each function was computed for both the u and v component of the wind field. As data point separation approaches zero

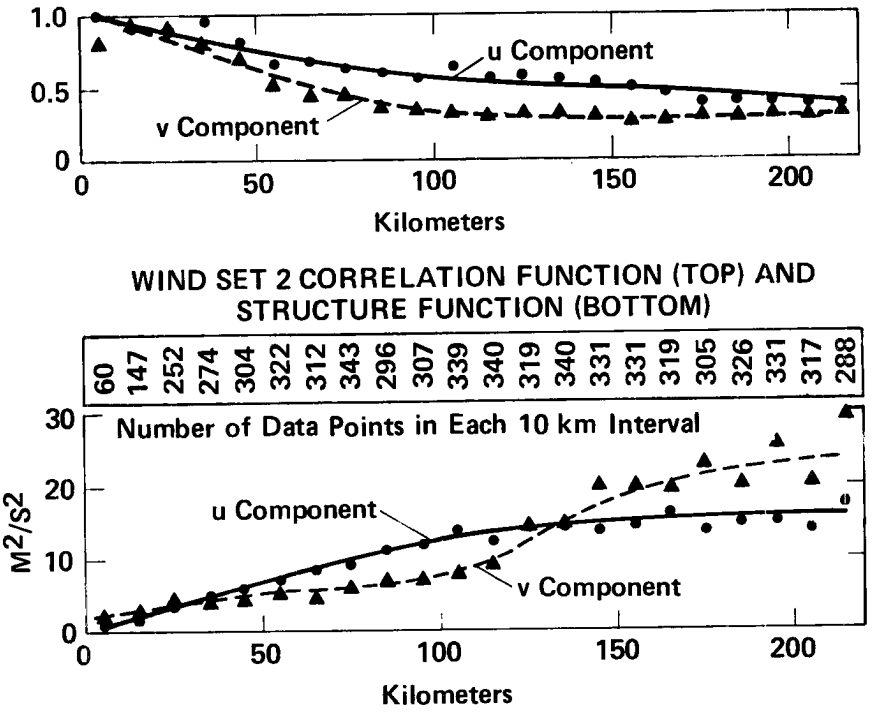

Figure 4.2 Correlation and structure functions for u and v components of the wind field shown in Figure 4.1. The number of data pairs whose separation distance fell in each 10 km interval is shown.

the structure function should approach twice the variances attributable to instrument and processing noise, and the correlation function should ideally approach unity. Thus, it seems that the low-level winds were determined very accurately in this specific case since both the u and v structure curves appear to approach zero. An analysis of many more cases is required before more quantitative calculations of the statistical "accuracy" of satellite measured winds may be made; but, these initial results seem promising.

The structure function plots also indicate that approximately 60% of the total variance in the u-component is occurring at scales of 50-135 km and in the v-component at scales of 100-150 km. The varying details of the structure of the two components of the wind indicates that different expressions might be needed for the respective correlation functions if an objective analysis scheme employing "optimal interpolations" were used. Nevertheless, the statistical analysis indicates that, for this particular case, the features of importance (those responsible for most of the variance) were of wavelength 150 km or less. This implies that, if the data were to be objectively gridded for additional study, a grid mesh of maximum spacing no greater than 0.5 degree latitude must be used.

Perhaps the primary reason that mesoscale weather phenomena, such as severe convective storms and squall-lines, are not better understood is that there is no distinct spectral gap separating small scale features from large scale features. With this problem in mind a structure analysis was performed upon a much larger satellite wind set (this data set was produced by NASA personnel and made available for study at CSU) obtained for a time only three and a half hours prior to that of the data shown in

Figure 4.1. The results of this computation are shown in Figure 4.3. This curve indicates that the total variance of the wind field is occurring primarily within two pronounced wavelength intervals--one on the synoptic scale and one on the mesoscale. Approximately 30% of the total variance is attributable to wavelengths of 600 to 800 km while the remaining 70% is at scales of less than 150 km. This indicates that relatively small mesoscale features probably played a crucial role in determining regions of storm development on this case study day.

The preliminary research done on structure analyses of satellite wind fields indicates that an expansion of this effort to include additional data sets might produce significant results that would affect not only mesoscale interpretation, objective analysis and diagnostic studies of satellite derived winds, but also results that would be directly applicable to other types of remotely and conventionally sensed meteorological data.

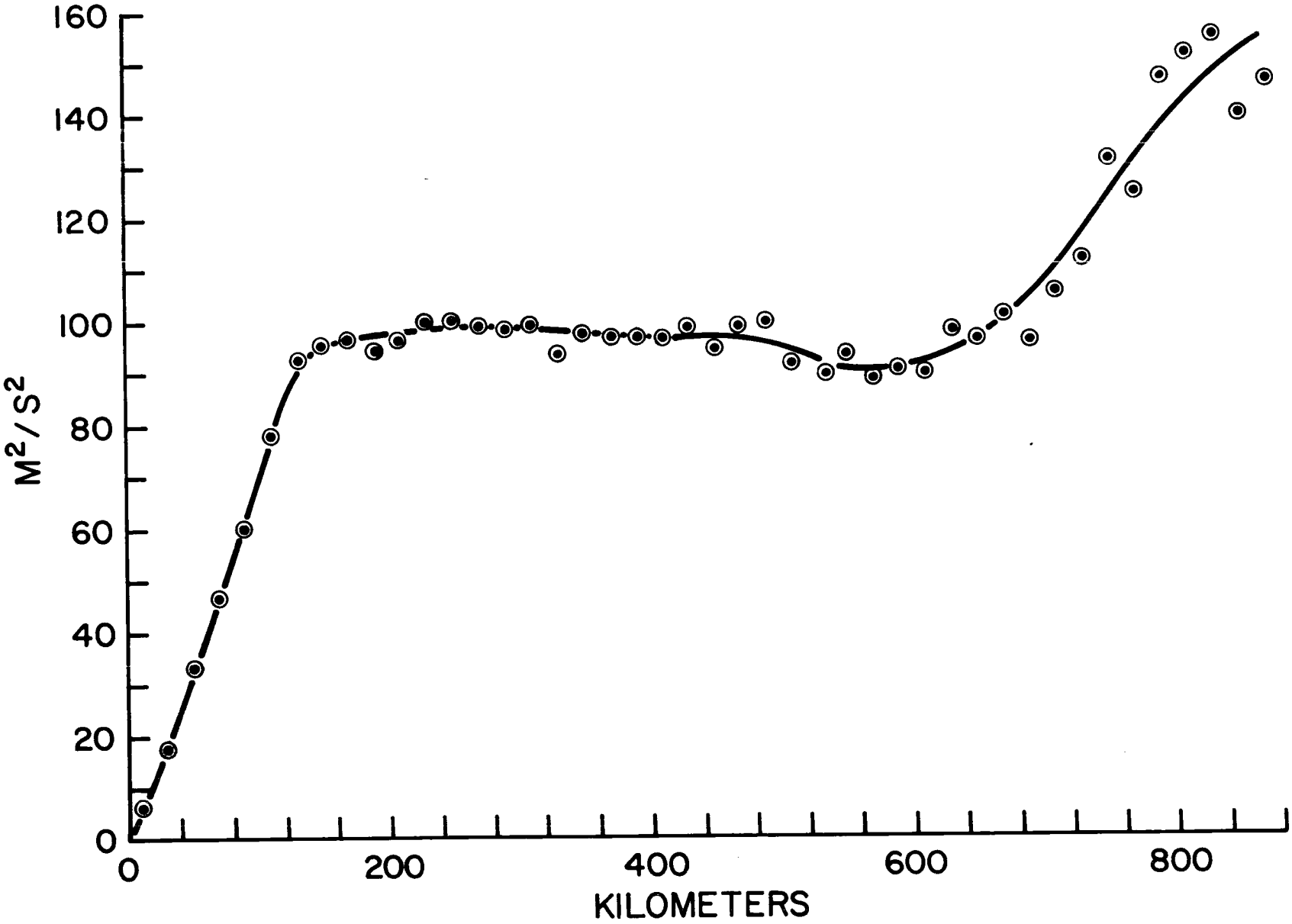

Figure 4.3 Structure function (u component) for satellite derived 1800 GMT wind set on 24 April 1975 (400+ vectors).

5.0 Analysis of the Pre-Convective Cloudiness - It's Relationship to Satellite Soundings and Severe Weather

5.1 Introduction

The purpose of this study was two-fold. The first question to be answered was to define satellite sounding capabilities in the pre-convective environment. These studies relate directly to the VTPR infrared sounder on the NOAA series of satellites. These studies may not be relevant to the second and third generation sounder system such as HIRS (High Resolution Infrared Sounder) systems and TOVS (Tiros Operational Vertical Sounder) whose resolution is almost twice that of the VTPR, and VAS (VISSR Atmospheric Sounder) which will be mounted on a geosynchronous satellite allowing half-hourly to hourly soundings to be made. Thus if the cloud fields are transient during one or two of the morning hours soundings can be made. At present there are no plans for instrumenting a vertical temperature sounder with microwave channels in the near future other then in the 50 GHz regions which has been used in the SCAMS (Scanning Microwave Spectrometer) on Nimbus 6 and the MSU (Microwave Sounding Unit) on TIROS-N. The instruments allow for soundings in a cloudy environment but only at three levels in the troposphere. The surface resolution is also between 100-150 km at subpoint which is fairly course for severe storm studies. These clouds will continue to be a problem for the infrared sounders for the next several years.

The second question to be answered was to determine the the pre-convective cloudiness could be related to the subsequent severe weather that afternoon, either by its areal extent, organization or the lack of cloudiness altogether.

The area chosen for this study was the Oklahoma, west Texas region. This coincides with the highest probability area of severe weather occurrences. The results may also be relevant to a future SESAME type program if one is to be forthcoming.

5.2 Data Analysis

The data used for this analysis consisted of SMS visible and infrared images for the months of April through June for the years 1975 and 1976. One mile resolution visible and equivalent 1 mile resolution IR images were used. A grid overlay was produced consisting of 45 boxes; 92x92 km on a side which could be placed on the 15 or 16Z morning visibile image to determine cloud cover (scattered, broken, overcast) in each of the boxes. The morning IR image was used to determine cloud type (low, middle, high). The late afternoon visible and infrared images (~2300-0000Z) were examined to locate areas where thunderstorms were developing. Figure 5.2.1 shows the grid box locations with respect to Oklahoma and the surrounding regions. This was placed on an acetate overlay at the same scale as the satellite images. Figure 5.2.2 shows a morning SMS-1 visible image taken at 1600Z or 1000 EST. Note the low-level broken cumulus field in the Texas panhandle region. Figure 5.2.3 is the matching infrared image showing this cloudiness as dark or warm. Figure 5.2.4 is the 2330Z enhanced infrared image for this same day and indicates that thunderstorms have developed in the area where the low-level cloudiness was that morning. This same technique was followed for all days available from April through June for the two years.

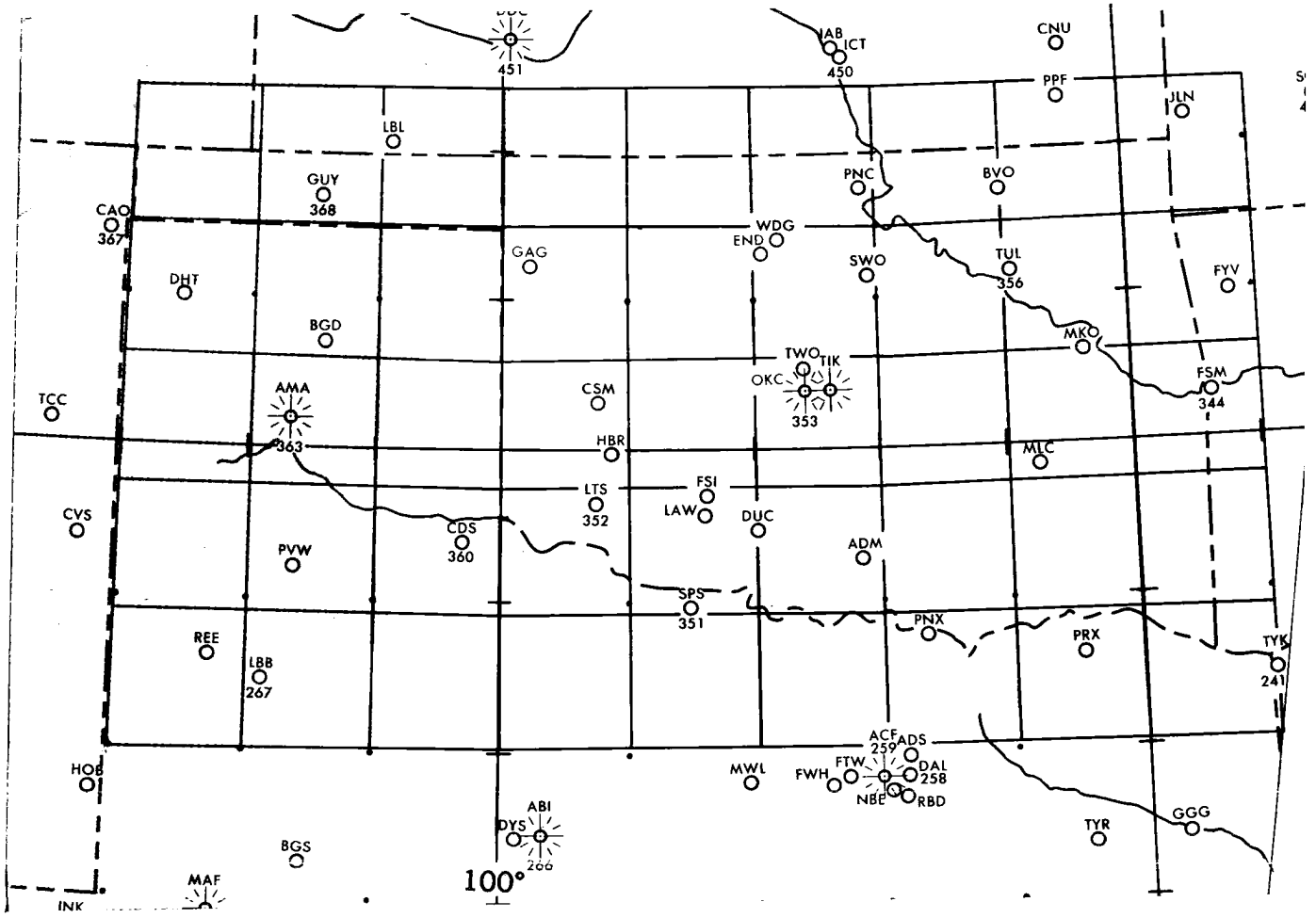

Figure 5.2.1 Grid bases over the Oklahoma region for which cloud climatology was performed.

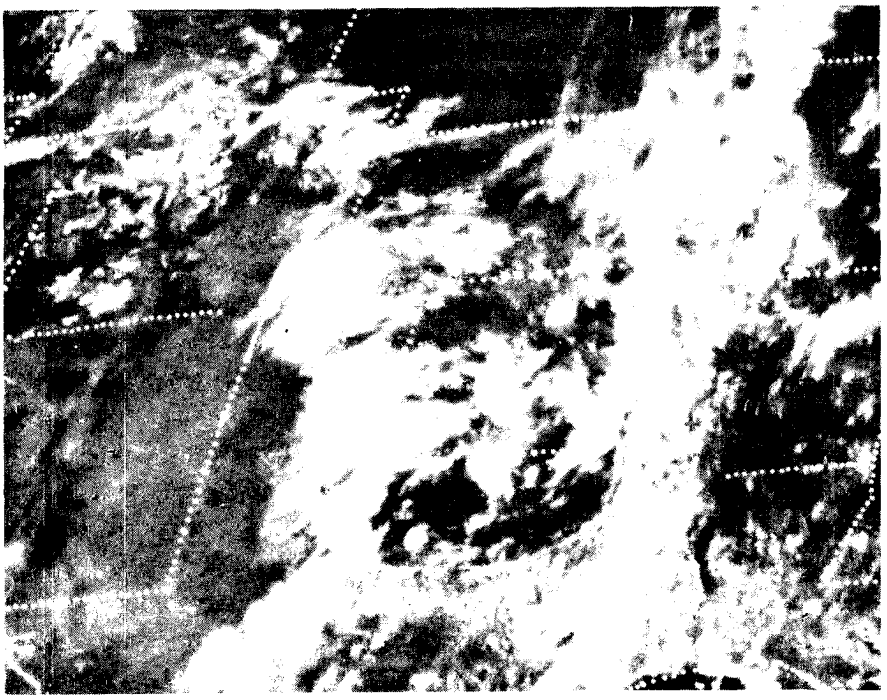

Figure 5.2.2 1600 GMT GOES-1 visible 1.85 km resolution image taken over the Oklahoma region. It was this type of image which was analyzed for this study.

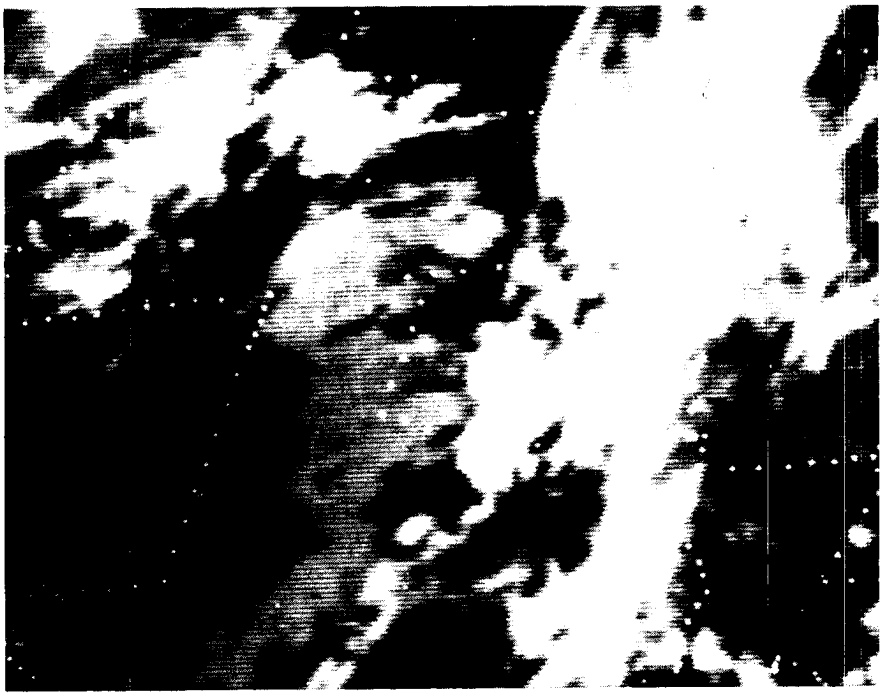

Figure 5.2.3 1600 GMT GOES-1 equivalent 1.85 km infrared image for 22 June 1976 used for this study to determine the approximate level of the clouds observed in the visible image.

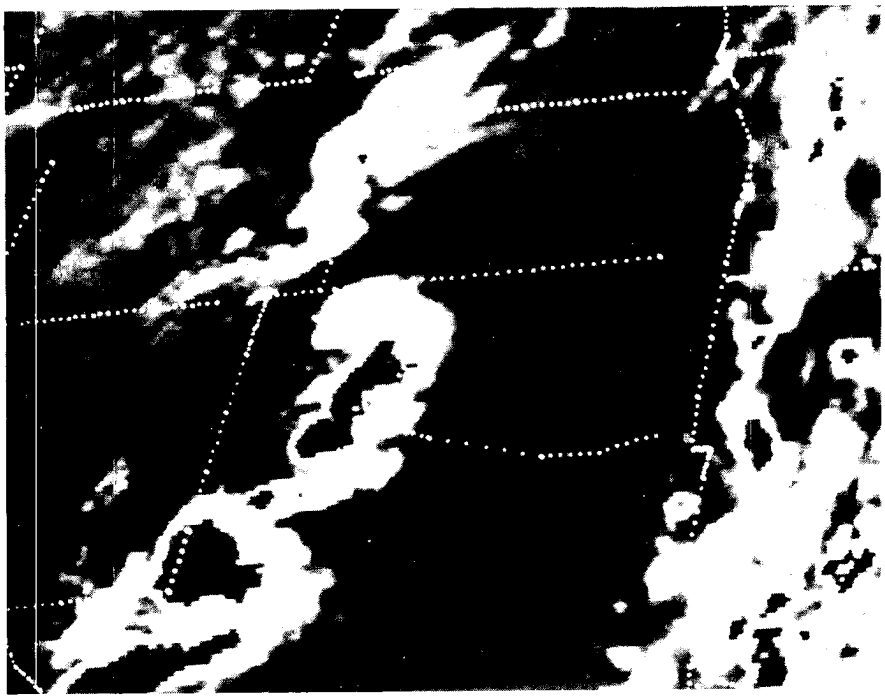

Figure 5.2.4 2330 GMT GOES-1 equivalent 1.85 km resolution enhanced infrared image for 22 June 1976 showing subsequent thunderstorm development in the Texas Panhandle region.

The severe weather reports for this study were taken from Storm Data published by the National Climatic Center. Severe weather reports were only used if they occurred before 03Z that evening. Each report was plotted on a map of the Oklahoma, west Texas region and compared to the morning cloudiness observed. Each of the 45 boxes was taken individually, therefore if more than one hail or tornado report was given per box, this only counted as one report. If more than one type of report i.e. hail and wind was reported in a single box these were counted as separate occurrences. The type of severe weather noted were hail, tornadoes, funnel clouds, damaging winds, and heavy rains.

5.3 Satellite Sounding Capabilities in the Pre-Storm Environment

For 1975 all 91 possible days for study were examined. For 1976 75 of the possible 91 days were available. Most of the missing days in 1976 were for April. If we break the data down by months we find the following results. Combining April 1975 and 1976 there were 8 severe weather days out of a possible 48 days we examined. Without exception each box where severe weather was reported had broken to overcast clouds in it during the morning hours (9-10 a.m. local). For all May's there were 24 severe weather days out of a possible 60 examined. Of these 24 days, 13 were either broken or overcast cloud cover in the location of the subsequent severe weather activity; 7 of the remaining days had completely clear skys and 4 had scattered clouds. For June there were 22 severe weather days out of a possible 58 days examined. Of these 22 severe weather days 6 had broken to overcast cloudiness; 9 of the remaining 22 days had completely clear skys and the other 7 scattered clouds. Table 5.3a summarizes these results and shows that 50% of the days with severe weather had broken to overcast sky cover making satellite soundings

difficult to impossible. The table shows this condition to be more prevelant in the April-May time period then in June indicating that in these early months, synoptic scale features are probably forcing the activity.

In Table 5.3b further analysis of the broken to overcast cloudy cases were performed and these were classified into low, middle or high cloudiness. The table shows that 7 of the 8 cases in April, 10 of the 13 cases in May and 3 of the 6 in June had high clouds. It is possible with the satellite sounder data to sound down to the cloud top. Thus for 5 of the 27 cases a sounding could have been made down to the top of the low-level cloud deck. Thus to restate the percentage of cases where satellite soundings could not be made on severe weather days would be 41%.

If we take each box individually rather than categorize by the days we find that for both years combined there were 152 severe weather reports within the 45 boxes. Of these, 58 were totally overcast, 33 had broken clouds, 30 had scattered clouds, and 31 had clear skies. Thus 60% of the boxes where severe weather occurred were obscured by clouds during the morning hours. However, there were boxes within the grid that had scattered to clear skies which could have been examined. Thus the 41% stated earlier is probably a better representation of the number of severe weather days where satellite soundings could not be made. (This should be improved when VAS is launched and the temporal capability of this system is utilized.)

5.4 Pre-Convective Cloudiness Related to Severe Weather

The results for this study were derived from the same data as used for the satellite sounding results. However, for this study we classified the cloudiness in each box to the type of severe weather observed. Table 5.4 summarizes all the severe weather reports for each box for the two years studied.

Table 5.4

Hail	Tornado	Funnel	Wind	Heavy Rain
22 CLR	2 CLR	4 CLR	3 CLR	2 BRK
17 SCT	4 SCT	6 SCT	3 SCT	2 OVC
14 BRK	5 BRK	8 BRK	6 BRK	
26 OVC	3 OVC	11 OVC	6 OVC	

As the table shows, hail dominates the severe weather reports. There are about as many clear cases as cloudy cases for hail. In a majority of these clear to scattered cloud cases the reports were either in west Texas or the clouds developed outside the region and advected in. In the other categories the broken to overcast cloudiness dominates and can be explained by the presence of large scale cloudiness due to synoptic scale forcing features. For most of the large scale outbreaks (more than 5 severe weather repots) all 45 boxes were covered with multilayered clouds. It also appears from this study that when only part of the 45 boxes were cloudy, the severe weather would occur in the cloudy boxes and not on the edge of the cloud system or in the clear air where surface heating might be expected to be stronger. Although this is far from being a quantitative study the observations made here show that the severe weather forms in the cloudy

regions possibly making use of the available moisture and the apparent vertical motion associated with cloudy regions. No apparent organization could be noted except for those cases where a large scale shortwave was affecting the area or strong surface fronts were noted on the surface chart. Then distinct lines and arcs could be noted even before convection developed. Finally, there was no apparent variation in severe weather days versus non-severe weather days by simply looking at the morning imagery unless a synoptic scale feature was present. Thus the imagery must be combined with the conventional meteorological data in most cases to help define potential severe weather locations.

Table 5.3a

	April	May	June	Totals	% of Total
# of Days Available	48	60	58	166	
# of Svr. Wx. Days	8	24	22	54	33%
OVC-BRK*	8	13	6	27	50%
SCT	0	4	7	11	20%
CLR	0	7	9	16	30%

Table 5.3b

		April	May	June
OVC-BRK		8	13	6
Maximum Cloud Height	Low	1	2	2
	Middle		1	1
	High	7	10	3

*Cloud cover for location of severe weather report and for a radius of 200 km for this location.

6.0 Collection of Three Minute Interval Satellite Digital Data During Severe Storm Outbreaks.

Through a joint effort by NESS, NASA and the U.S. Army this past spring a unique data set was gathered from the GOES-1 satellite consisting of ten days during severe weather events where 3 minute interval data were gathered from 1700Z - 0100Z. Table 6.1 lists six of these days which were particularly interesting.

Table 6.1

RRSD	3 Minute Data Period (GMT)	Recorded at WSMR	Remarks
4 April	1700-2000	1700-2000Z	After 2000Z went to 7.5 min data
5 May	1700-0100	1730-2330Z	
15 May	1730-2300	1730-2300Z	
18 May	1700-0100	1700-0100Z	
20 May	1700-0100	1700-0100Z	
27 May	1700-0100	1700-0100Z	

Both Reynolds and Vonder Haar were designated user's of this data set during the initial planning discussion for the RRSD's. This was done to demonstrate to NESS and NASA that there was an urgent need for these types of measurements to be made and that research use would be made of the data if it became available. Close cooperation between NESS-CSU-WSMR made the successful recording of the digital data possible.

Along with the rapid scan digital satellite data other researchers were collecting supporting data. Dr. Fujita at the University of Chicago made special areal surveillance flights near tornado bearing thunderstorms, as well as the damage paths caused by these storms. Researchers at NSSL were collecting routine Doppler radar data for the Oklahoma region during May as well as taking special surface and upper-air data at high temporal and spatial frequencies.

We hope to make this data set the foundation for a second year of study in satellite applications of severe storms. As we have demonstrated in this report, the temporaral frequency is critical in this type of work. It is thus imperative that detailed studies be made using this data for it should have strong implications to future satellite applications as well as designs of new satellite instruments.

7.0 Summary and Recommendations

In this first year of study under Grant ATM76-21307 we have tried to demonstrate the need for quantifying available satellite information into parameters that not only can be compared to other conventional data sources but comparable to other researcher's satellite observations as well. We have developed a new "figure of merit" for the satellite sounder data. One that can be used to assess its use at the mesoscale.

The satellite sounder data has been used to demonstrate that in the horizontal, mesoscale perturbations can be observed and that moisture differences generally occur on a smaller scan than thermal differences. These results are consistent with results from the NSSL RAOB network analyzed for the same days and times as the satellite sounder data. Preliminary indications are that severe vs. non-severe weather days may also be indicated by the magnitude of the "structure" of the moisture and temperature in the pre-convective environment.

These results are encouraging and should be further substantiated by another season of satellite-RAOB mesoscale moisture, temperature comparisons. We would hope this could be done this next spring if NSSL continues its RAOB program.

Studies of the pre-convective cloudiness have shown that on approximately half the days where severe weather of some kind occurs, there is enough clear area for soundings to be made by satellites. For the two years of data that went into this study there was no strong relationship between morning cloudiness and subsequent severe weather. It appeared that for most severe weather events that the morning skies in the vicinity of the event were covered by broken to overcast cloudiness. Only on days of large scale synoptic forcing could cloud organization be seen. These days also

had most of the more organized severe weather.

Through the use of geosynchronous digital satellite data it was demonstrated that through tracking of low-level cloud motions, quantitative estimates of convergence, vorticity and moisture convergence near the severe weather could be derived. Through statistical methods it was shown that variations in the wind field occur on short space and time intervals. Thus accuracy in the wind measurements are crucial if one is to observe those features causing the severe weather to develop.

Further analysis of the digital satellite data showed IR growth rates may indicate those convective clouds which cause severe weather. The rapid expansion of colder isotherm areas on cloud top denote the severity, even though the absolute magnitude of the top-temperatures may be underestimated by the satellite.

Much more work is needed in this area. Through this grant we were able to collect the best satellite data sets to date containing three minute interval GOES-1 digital data. These high frequency data along with supporting rawinsonde, radar and some aircraft data should help substantiate the results shown here. It is critical that some sort of "cloud truth" data (i.e. aircraft observed cloud heights or RHI data) be made available to these types of studies, and we feel this next year of study will have this information for comparison. There are plans at the present time to have a second season of rapid scan data taken from GOES-1. It is possible that with our active role in the planning and data gathering phase (CSU will have a Direct Readout Ground Station for collecting digital SMS/GOES data by this spring) that better cloud truth data as well as other supporting data can be collected.

8.0 BIBLIOGRAPHY

Adler, R. F. and D. D. Fenn, 1976: Thunderstorm monitoring from a geosynchronous satellite. Preprint of Seventh Conf. on Aerospace and Aeronautical Meteorology and Symposium on Remote Sensing from Satellites, AMS, Melbourne, Florida, 307-311.

Adler, R. F. and D. D. Fenn, 19-7: Satellite-based thunderstorm intensity parameters. Preprint of Tenth Conf. on Severe Local Storms, AMS, Omaha, Nebraska, 8-15.

Barnes, S. L., 1977: Personal communication, correlation results from 1976 NSSL rawinsonde data.

Barnes, S. L. and D. K. Lilly, 1975: Covariance Analysis of Severe Storm Environments, Reprints, Ninth Conference on Severe Local Storms, pp. 301-306.

Billingsley, J. B., 1976: Interactive image processing for meteorological applications at NASA/GSFC. Preprint of Seventh Conf. on Aerospace and Aeronautical Meteorology and Symposium on Remote Sensing from Satellites, AMS, Melbourne, Florida, 268-275.

Conrath, B. M., 1972: Vertical Resolution of Temperature Profiles Obtained from Remote Radiation Measurements, J. Atmos. Sci., 29 pp. 1262-1271.

Fujita, T. T., 1973: Proposed mechanism of tornado formation from rotating thunderstorm. Preprint of Eight Conf. on Severe Local Storms, AMS, Denver, Colorado, 191-196.

Fujita, T. T., E. W. Pearl and W. E. Shenk, 1975: Satellite tracked cumulus velocities. J. Appl. Meteor., 32, 407-413.

Gandin, L. S., 1963: Objective Analysis of Meteorological Fields, Translated from Russian, Israel Program for Scientific Translations, Jerusalem, 242 pp.

Hasler, A. F., W. E. Shenk, and W. C. Skillman, 1976: Wind estimates from cloud motions: phase 1 of an in situ aircraft verification experiment. J. Appl. Meteor., 15, 10-15.

Hillger, D. W. and T. H. Vonder Haar 1976: Mesoscale Temperature and Moisture Fields from Satellite Infrared Soundings. Atmospheric Science Paper No. 249, Colorado State University, Fort Collins, Colorado, 66 pp.

Hillger, D. W. and T. H. Vonder Haar, 1977: Deriving Mesoscale Temperature and Moisture Fields from Satellite Radiance Measurements over the United States, J. Appl. Meteor., 16, pp. 715-726.

Maddox, R. A., A. J. Negri and T. H. Vonder Haar, 1977: Analysis of satellite derived winds for 24 April 1975. Preprint of Tenth Conf. of Severe Local Storms, AMS, Omaha, Nebraska, 54-60.

McMillin, L. M., D. Q. Wark, J. M. Siokajlo, P. G. Abel, A. Werbowetzki, L. A. Lauritson, J. A. Pritchard, D. S. Crosby, H. M. Woolf, R. C. Luebbe, M. P. Weinreb, H. E. Fleming, F. E. Bittner and C. M. Hayden, 1973: Satellite Infrared Soundings from NOAA Spacecraft. NOAA Tech. Report, NESS 65, Sept., 112 pp.

Negri, A. J., 1977: Satellite Observations of the Onset and Growth of Severe Local Storms, Atmospheric Science Paper No. 278, Colorado State University, Fort Collins, CO, 89 pp.

Negri, A. J., D. W. Hillger and T. H. Vonder Haar, 1977: Moisture convergence from a combined mesoscale moisture analysis and wind field for 24 April 1975. Preprint of Tenth Conf. on Severe Local Storms, AMS, Omaha, Nebraska, 48-53.

Negri, A. J., D. W. Reynolds and R. A. Maddox, 1976: Measurements of cumulonimbus clouds using quantitative satellite and radar data. Preprint of Seventh Conf. on Aerospace and Aeronautical Meteorology and Remote Sensing from Satellites, AMS, Melbourne, Florida, 119-124.

Otto-Bliesner, B., D. P. Baumhefner and T. W. Schlatter, 1976: A comparison of several meteorological analysis schemes over a data-rich region. Preprints, Sixth Conf. on Weather Analysis and Forecasting, AMS, Albany, NY, 191-195.

Purdom, J. F. W., 1976a: Tornadic thunderstorms and GOES satellite imagery. Paper presented at Ninth Conf. on Severe Local Storms, AMS, Norman, Oklahoma, 5 p.

Rodgers, C. D., 1976: The Vertical Resolution of Remotely Sounded Temperature Profiles with a Priori Statistics, J. Atmos. Sci., 33 pp. 707-709.

Sasaki, Y. K., 1973: Mechanism of squall line formation as suggested by variational analysis of hourly surface observations. Preprint of Eighth Conf. on Severe Local Storms, AMS, Denver, Colorado, 300-307.

Sasaki, Y. K., 1975: Variational analysis and dynamics of severe local storms. Final report submitted to NOAA, U.S. Department of Commerce, Boulder, Colorado.

Schlatter, T. W., 1975: Some experiments with a multivariate statistical objective analysis scheme. Mon. Wea. Rev., 103, 246-257.

Scofield, R. A. and V. J. Oliver, 1977: A scheme for estimating convective rainfall from satellite imagery. NOAA Tech. Mem., NESS 86, 47 p.

Suchman, D. and D. W. Martin, 1976: Wind sets from SMS images: An assessment of quality for GATE. J. Appl. Meteor., 15, 1265-1278.

Thiebaux, H. J., 1975: Experiments with correlation representations for objective analysis. Mon. Wea. Rev., 103, 617-627.

Thompson, O. E., J. K. Eom, and J. R. Wagenhofer, 1976: On the Resolution of Temperature Profile Finestructure by the NOAA Satellite Vertical Temperature Profile Radiometer, Mon. Wea. Rev., 104, pp. 117-126.

Wilson, G. S., 1976: Large-scale vertical motion calculations in the AVE IV experiment. Geophysical Research Letters, 3, 735-738.

9.0 STUDENTS WHOLLY OR PARTIALLY SUPPORTED UNDER GRANT ATM76-21307

Andrew J. Negri - M.S.
Donald W. Hillger - Ph.D.
Robert A. Maddox - Ph.D.
Young P. Yee - M.S.
Steven Pryor - M.S. AFIT Student

10.0 THESIS TITLES

Negri, A. J. (1977) Satellite Observations of the Onset and Growth of Severe Local Storms. M.S. Thesis, Dept. of Atmospheric Science, Colorado State University, Fort Collins, 89 pp.

11.0 LIST OF FIGURES

BIBLIOGRAPHIC DATA SHEET	1. Report No. CSU-ATSP-290	2.	3. Recipient's Accession No.
4. Title and Subtitle SATELLITE STUDIES OF SEVERE CONVECTIVE STORMS			5. Report Date June 1978 6.
7. Author(s) David W. Reynolds and Thomas H. Vonder Haar			8. Performing Organization Rept. No. 290
9. Performing Organization Name and Address Atmospheric Science Department Colorado State University Fort Collins, CO 80523			10. Project/Task/Work Unit No. 11. Contract/Grant No. NSF ATM76-21307
12. Sponsoring Organization Name and Address National Science Foundation Washington, D.C. 20550			13. Type of Report & Period Covered Final Report 14.

15. Supplementary Notes

16. Abstracts Results are reported in the analysis of the pre-severe and severe storm environment using meteorological satellite data. Using polar-orbiter vertical temperature sounder data and applying statistical methods, determination of the scale and intensity of pre-severe storm temperature and moisture gradients have been examined. Results show that strong moisture gradients at the 100-200 km scale and temperature gradients at the 200-400 km scale are precursors to severe weather events.

Through the use of satellite derived low level wind vectors, combined with surface moisture values, results have shown some skill in relating areas of high moisture convergence with subsequent severe weather. These low-level wind vectors have also been used independently to derive low level convergence and vorticity patterns at the mesoscale in the pre-storm environment. A statistical examination was performed on the derived winds to examine their accuracy and the scale needed to be able to define the severe weather environment. These results show that the features of importance occur at two separate wavelengths, 150 km or less, and 600-800 km. Thus both mesoscale and synoptic scale forcing features are significant to severe weather development, at least on the days examined here. Once the severe weather has developed, the rate of growth of the cloud, as determined by decreasing in cloud top temperature, is related to the timing of the severe weather event.

Preliminary results from a cloud climatology performed over Oklahoma for the April-June period using two years of SMS/GOES data are reported. The pre-convective cloudiness is examined during the morning hours (1000 LT) to determine how it effects satellite sounder capabilities and subsequent severe weather occurrence. On 41% of severe weather days, no satellite sounder information cloud have been made due to overcast cloudiness. On the majority of the severe weather days examined, the convective clouds formed over the areas having morning cloudiness rather than in the clear air or at cloud-clear boundaries. This is explained by the fact that the clouds represent areas of moisture and vertical motion conducive to convective development.

17. Key Words

Satellite studies, severe storms

17c. COSATI Field/Group

18. Availability Statement	19. Security Class (This Report) UNCLASSIFIED	21. No. of Pages 69
	20. Security Class (This Page UNCLASSIFIED	22. Price